Solutions to the questions

Chapter 1

1.1 The positive and negative signs are a consequence of wave character of the electron. The signs of the wave functions change with a certain frequency. They have no effect on the probability density of finding an electron at a certain place because negative signs are cancelled out by the multiplication

$$P(x,y,z) = \Psi^*(x,y,z)\Psi(x,y,z).$$

1.2 The wavenumber is directly linear proportional to the energy. As a consequence a spectrum given in wavenumbers reflects directly the energy differences between the various states of a molecule. Also, the wavenumber of a transition including electronic and vibrational excitation can be simply calculated from the sum of the wavenumbers for the pure electronic and vibrational transitions. The presentation of spectral data on a wavelength scale always requires calculating the corresponding energies from the inverse of the wavelength.

1.3

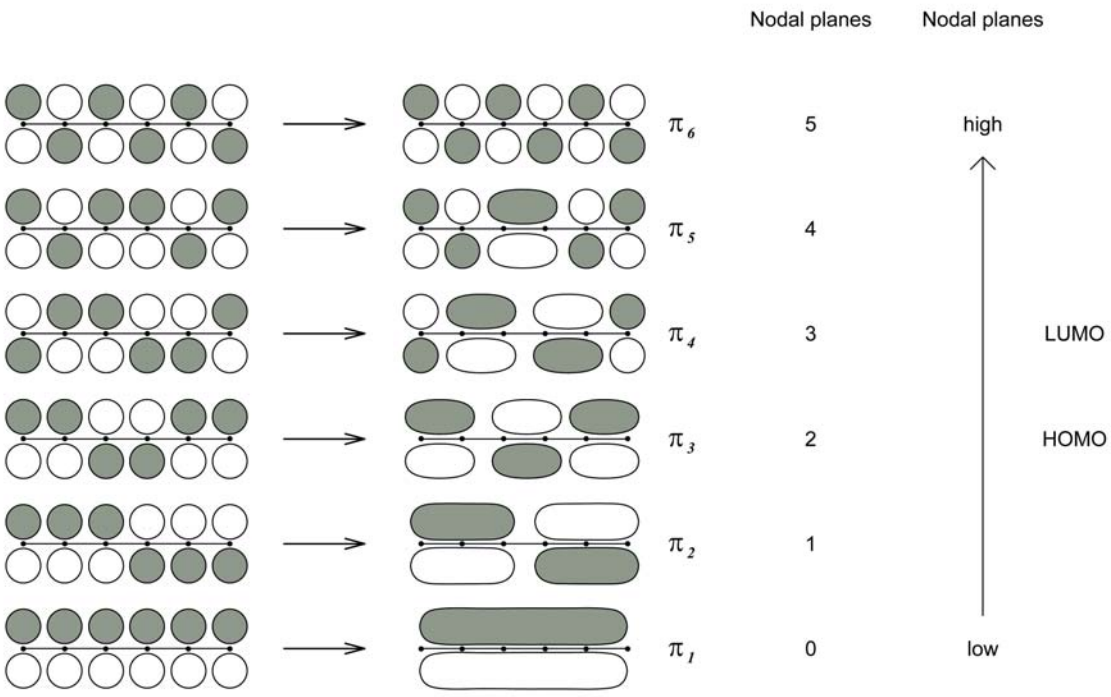

Modern Biophysical Chemistry. Detection and Analysis of Biomolecules. Peter Jomo Walla

ISBN: 978-3-527-32360-9

1.4 (a) The photon must have the correct energy that equals to the energy difference between the final electronic state and the initial electronic state.

(b) The transition between the two states is dipole allowed.

(c) The direction of the oscillation of the electric field of light fits with the transition dipole moment.

1.5 The transition dipole moment lies within in the plane of the molecule perpendicular with respect to the long molecular axis (see figure):

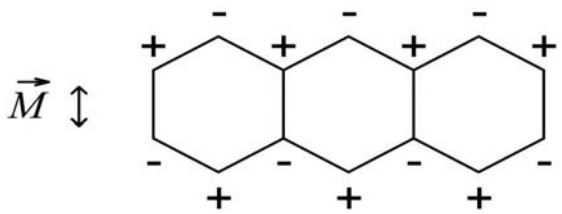

1.6

Using Laporte's rule this question can be answered based on the symmetry of the orbitals:

(a) The $\pi_1 \rightarrow \pi_4^*$ transition corresponds to a transition between orbitals with the parities u → g and is therefore dipole allowed.
(b) The $\pi_1 \rightarrow \pi_3^*$ transition corresponds to a transition between orbitals with the parities u → u and is therefore dipole forbidden.
(c) The $\pi_2 \rightarrow \pi_3^*$ transition corresponds to a transition between orbitals with the parities g → u and is therefore dipole allowed.

1.7 (a) The solvent environment. Depending on the statistical positions and orientations of solvent molecules around individual absorbing or emitting molecules their corresponding state energies and thus transition energies are increased or decreased, leading to the observation of a line broadening. In more polar solvents, electronic states that are more polarizable are often energetically lowered to a larger extent. Since excited states are often more polarizable, a redshift is often observed in more polar solvents.

(b) The nuclear geometry of molecules in the electronic excited state and the electronic ground state. According to the Franck–Condon principle, during an electronic excitation the simultaneous excitation of those vibrational states is the most probable for which the nuclear geometry can remain similar to that in the electronic ground state.

1.8 Like orbitals changing signs at regions corresponding to zero probabilities of finding the electron, vibrational wavefunctions also change their sign at regions corresponding to zero probabilities of finding the nuclei (see figure below):

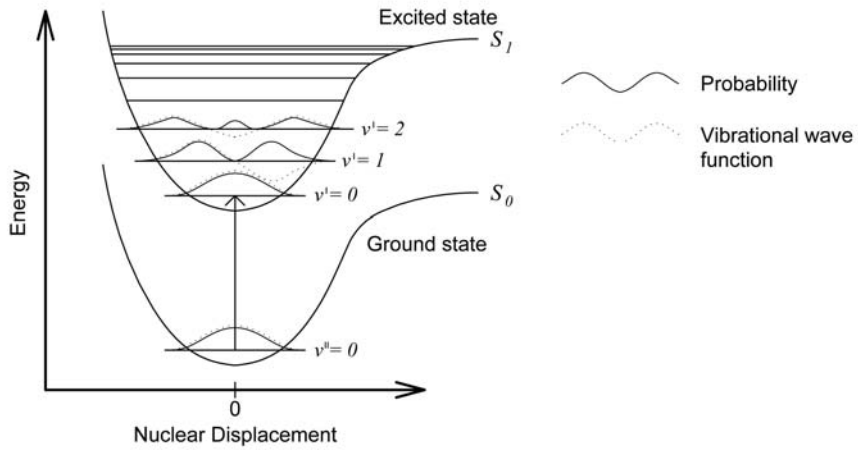

1.9 Fluorescence

(a) The rate for fluorescence and thus the fluorescence quantum yield is the larger the larger the transition dipole moment between S_1 and S_{0i} is. This is often the case for molecules with extended conjugated π-systems.

(b) A larger energy gap between S_1 and S_0 often results in a smaller probability for radiationless deactivation by internal conversion into a highly vibrational state of S_0. As a consequence the fluorescence quantum yield is higher.

(c) Rigid molecular structures also often result in smaller probabilities for radiationless deactivation and thus higher fluorescence quantum yields.

Internal conversion

(a) A small energy gap between S_1 and S_0 often results in larger rates for internal conversion because the probability of greater overlap of the vibrational wavefunctions of ground and excited states is higher.

(b) A flexible molecular structure also supports a radiationless internal conversion since the electronic excitation energy can then be more easily converted into high vibrational excitation.

(c) Also, molecules in higher electronically excited states, S_2, S_3…, are usually deexcited to S_1 by internal conversion because of the smaller energy gaps between these electronically excited states.

Intersystem crossing

(a) Intersystem crossing requires a mechanism that compensates the electrons spin flip (e.g., by spin–orbital coupling).

(b) In addition all factors that enhance internal conversion are also important for intersystem crossing. For example, a good overlap between vibrational wave functions of S_1 and the vibrational wave functions of the T_1 also increases the probability for intersystem crossing.

1.10

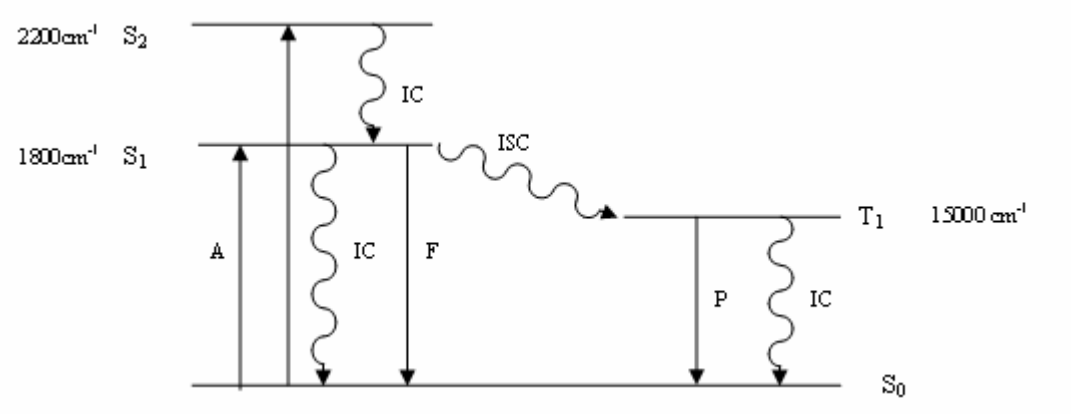

The wavelength necessary for an $S_0 \rightarrow S_1$ excitation is:

$$\frac{1}{\lambda_{S_0 \rightarrow S_1}} = 18000\,\text{cm}^{-1}$$

$$\lambda_{S_0 \rightarrow S_1} = 555\,\text{nm}$$

The wavelength necessary for an $S_0 \rightarrow S_2$ excitation is:

$$\frac{1}{\lambda_{S_0 \rightarrow S_2}} = 22000\,\text{cm}^{-1}$$

$$\lambda_{S_0 \rightarrow S_2} = 454\,\text{nm}$$

(a)

$$\tau_{\text{state}} = \left(\sum k_x\right)^{-1}$$

$$\tau_{S_1} = \left({\tau_{Fl}}^{-1} + {\tau_{IC}^{S}}^{-1} + {\tau_{ISC}}^{-1}\right)^{-1} = \left(5\,\text{ns}^{-1} + 25\,\text{ns}^{-1} + 100\,\text{ns}^{-1}\right)^{-1}$$

$$\tau_{S_1} = \left(\tfrac{1}{5} + \tfrac{1}{25} + \tfrac{1}{100}\right)^{-1}\,\text{ns} = 4\,\text{ns}$$

(b)

$$\Phi_{Fl} = \frac{k_{Fl}}{k_{Fl} + k_{IC}^{S} + k_{ISC}} = \frac{{\tau_{Fl}}^{-1}}{{\tau_{Fl}}^{-1} + {\tau_{IC}^{S}}^{-1} + {\tau_{ISC}}^{-1}} = \frac{5\,\text{ns}^{-1}}{5\,\text{ns}^{-1} + 25\,\text{ns}^{-1} + 100\,\text{ns}^{-1}} = 0.8$$

(c)

$$\Phi_{\text{Triplet}} = \frac{k_{ISC}}{k_{Fl} + k_{IC}^{S} + k_{ISC}} = \frac{{\tau_{ISC}}^{-1}}{{\tau_{Fl}}^{-1} + {\tau_{IC}^{S}}^{-1} + {\tau_{ISC}}^{-1}} = \frac{100\,\text{ns}^{-1}}{5\,\text{ns}^{-1} + 25\,\text{ns}^{-1} + 100\,\text{ns}^{-1}} = 0.04$$

(d)

$$\tau_{\text{state}} = \left(\sum k_x\right)^{-1}$$

$$\tau_{\text{Triplet}} = \left(k_{\text{ph}} + k_{\text{IC}}^{\text{T}\to\text{S}}\right)^{-1} = \left(\tau_{\text{ph}}{}^{-1} + \tau_{\text{IC}}^{\text{T}\to\text{S}-1}\right)^{-1} = \left(2\,\text{s}^{-1} + 20\,\mu\text{s}^{-1}\right)^{-1} = 20\,\mu\text{s}$$

(e)

$$\Phi_{\text{ph}} = \Phi_{\text{Triplet}}\,\frac{k_{\text{ph}}}{k_{\text{ph}} + k_{\text{IC}}^{\text{T}\to\text{S}}} = 0.04 \cdot \frac{\tau_{\text{ph}}{}^{-1}}{\tau_{\text{ph}}{}^{-1} + \tau_{\text{IC}}^{\text{T}\to\text{S}-1}} = 0.04 \cdot \frac{2\,\text{s}^{-1}}{2\,\text{s}^{-1} + 20\,\mu\text{s}^{-1}} = 4\times10^{-7}$$

Chapter 2

2.1

$$\mathrm{OD}(550\,\mathrm{nm}) = \log\frac{I_0(550\,\mathrm{nm})}{I(550\,\mathrm{nm})} = \log\frac{I_0}{0.8I_0} = \log 1.25 = 0.097$$

$$\mathrm{OD}(550\,\mathrm{nm}) = \varepsilon(550\,\mathrm{nm}) \times c \times l$$

$$0.097 = 20000\,\mathrm{M^{-1}\,cm^{-1}} \times c \times 1\,\mathrm{cm}$$

$$c = 4.8 \times 10^{-6}\,\mathrm{M}$$

2.2 The fluorescence intensity is proportional to the concentration of the compound.
Fluorescence intensity of the first sample = I.
Fluorescence intensity of the second sample = ½I:

$$\frac{I}{0.5I} = \frac{4.8 \times 10^{-6}\,\mathrm{M}}{c}$$

$$c = 2.4 \times 10^{-6}\,\mathrm{M}$$

The artefact we have to consider is potential reabsorption of the emitted fluorescence by the compound itself. The fluorescence intensity varies linearly with concentration at low concentrations. At high concentrations, however, reabsorption occurs and the observed fluorescence is smaller than that corresponding to a linear relationship with the concentration.

2.3 Tryptophan possesses the largest conjugated π-electron system. This results in the longest absorption wavelength. The large conjugated π-electron system also results in the largest transition dipole moment. As a consequence tryptophan has a larger extinction coefficient and fluorescence quantum yield than the two other aromatic amino acids. Tyrosine usually dominates the fluorescence properties of proteins due to its frequent occurrence in proteins.

2.4 Because $Q = \mathrm{OD}(260\,\mathrm{nm}) / \mathrm{OD}(280\,\mathrm{nm}) = 1.8$ the sample is pure double-stranded DNA.

The optical density at 260nm id OD(260) = Q.OD(280) = 0.18

According to the Beer–Lambert law it concentration is:

$$OD(\lambda) = \varepsilon(\lambda) \times c \times l$$
$$\Rightarrow OD(\lambda) \; \alpha \; c$$
$$\frac{1.0OD(260\mathrm{nm})}{0.18OD(260\mathrm{nm})} = \frac{50mg/l}{c}$$
$$c = 9mg/l$$

2.5 In the cold, the blood circulation in the bodies extremities is decreased to avoid the loss of heat. As a consequence the blood in the extremities, including the lips, is less saturated with oxygen. The result is a more bluish colour of haemoglobin that can be seen at the lips.

2.6 Cooperativity occurs in cases in which the binding of a ligand to one receptor of a multimer protein alters the affinity of the other receptors to the ligands. The mechanism is often based on conformational changes induced by the binding. For example, if the first oxygen has bound to a free haemoglobin subunit, the binding affinity for the other subunits increases by a conformational change. This is called positive cooperativity. Cooperativity is very important for biology because it keeps the metabolites within certain tolerable concentration limits.

2.7 Chlorophylls contain two major absorption bands, one in the blue or near-UV region and one in the red or near-IR region. The lack of a significant absorption in the green region gives chlorophylls their characteristic green or blue-green colour. Carotenoids exhibit an intense absorption band in the 400–500 nm region, giving them the characteristic orange colour.

Chlorophylls are the most abundant pigments in plants in summer. Consequently, plant leaves in summer exhibit a green colour. But in fall the chlorophylls decompose and only carotenoids remain in the leaves. This is why plant leaves in the fall are orange.

Chapter 3

3.1

$$\Phi_{\mathrm{Fl}} = \frac{k_{\mathrm{Fl}}}{k_{\mathrm{Fl}} + k_{\mathrm{IC}}^{\mathrm{S}} + k_{\mathrm{ISC}}} = \frac{\tau_{\mathrm{Fl}}{}^{-1}}{\tau_{\mathrm{Fl}}{}^{-1} + \tau_{\mathrm{IC}}^{\mathrm{S}\,-1} + \tau_{\mathrm{ISC}}{}^{-1}}$$

Label A:

$$\Phi_{\mathrm{Fl}} = \frac{5\,\mathrm{ns}^{-1}}{5\,\mathrm{ns}^{-1} + 25\,\mathrm{ns}^{-1} + 100\,\mathrm{ns}^{-1}} = 0.8$$

Label B:

$$\Phi_{\mathrm{Fl}} = \frac{5\,\mathrm{ns}^{-1}}{5\,\mathrm{ns}^{-1} + 25\,\mathrm{ns}^{-1} + 20\,\mathrm{ns}^{-1}} = 0.69$$

A high fluorescence quantum yield is necessary for a sensitive detection of fluorescence markers. As a consequence Label A is the better fluorescent label. In addition, it has a smaller probability of forming a triplet states and the triplet state lifetime is shorter.

In addition, it is important that a good fluorescent label is:
(a) sufficiently soluble in physiological aqueous environment;
(b) has chemically active side chains that allow a non-aggressive but still effective labelling of biomolecules;
(c) shows high photostability.

3.2 It is better to choose the labelling position remote from the active site of biomolecules so as not to interfere with binding affinities and enzyme kinetic constants. However, the binding site must also be chosen in a way that donor and acceptor dye are close enough for an effective Förster energy transfer in the case of the assumed binding mechanism. To achieve the labelling at sites that fulfil both requirements one would chose thiol group reactive labels. Then the specific labelling sites can be obtained by point mutation at the corresponding positions in the DNA. By point mutation undesired cysteine sites can be removed and desired cysteine sites can be artificially added.

3.3 The organisms can be cloned in such a way that they express the protein of interest as fusion-proteins with GFP. The GFP can be used as fluorescence marker. This allows the observation of the distribution of this protein in the living organisms by fluorescence microscopy.

3.4 Introducing sequences of histidines into proteins represent a his-tag. This tag is based on the high affinity of Ni^{2+} ion for several histidine residues in a row. Ni^{2+} ions can then be immobilized to a solid matrix, for example by nitrilotriacetic acid residues. Ni^{2+} ions coordinate with the proteins with histidine residues as a means of purifying them.

3.5 1 nM streptavidin has four binding sites:

Biotin	+ Binding sites of streptavidin	↔ streptavidin–biotin complex:
	4 nM	
x	4 nM	
x–2 nM	2 nM	2nM

The binding affinity $K_a = \dfrac{[\text{avidin} - \text{biotin}]}{[\text{biotin}] \times [\text{monomer}]} = 10^{13}\ \text{M}^{-1}$

$$K_a = \frac{2\,\text{nM}}{(x - 2\,\text{nM}) \times 2\,\text{nM}} = 10^{13}\ \text{M}^{-1}$$

$$x - 2\,\text{nM} = 10^{-13}\ \text{M}$$

$$x = 2\,\text{nM} + 10^{-4}\ \text{nM} \approx 2\,\text{nM}$$

3.6

The anisotropy of the mixed solution is a linear combination of r_B and r_F:

$$\bar{r} = 0.1 = f_F \times r_F + f_B \times r_B = f_F \times 0.07 + f_B \times 0.2$$

$$f_B = \frac{\bar{r} - r_F}{r_B - r_F} = 0.2308 \quad f_F = 1 - f_B = 0.7692$$

If 1nM solutions are mixed in equal parts, the resulting concentration is 0.5nM. At equilibrium $0.5nM \times f_B = 0.3846nM$ are bound and $0.5nM \times f_F = 0.1154nM$ are free.

Dissociation constant $K = \dfrac{[labelled \quad ligand][receptor]}{[label - receptor]}$

$$K = \frac{0.1154nM \times 0.1154nM}{0.3846nM} = 1.28nM$$

The Dissociation constant is K=1.28 nM.

3.7

(a) $r_0 = 0.4 \times \left(\dfrac{3\cos^2 \alpha - 1}{2} \right)$

$$r_0 = 0.4 \times \left(\frac{3\cos^2 20^o - 1}{2} \right) = 0.33$$

The fluorescence anisotropy observed for the free ligand is:

$$\bar{r} = \frac{\gamma_0}{1 + \tau_{S1} / \Phi} = \frac{0.33}{1 + 9\,\text{ns} / 1\,\text{ns}} 0.033$$

(b) The rotational correlation time of the receptor–ligand complex:

$$\varphi \approx \frac{\eta V}{RT} = \frac{\eta M}{RT}\left(\bar{\nu} + h\right) = \frac{0.89\times10^{-3}\,\text{kg m}^{-1}\,\text{s}^{-1}\times 20000\,\text{g mol}^{-1}}{8.31441\,\text{J K}^{-1}\,\text{mol}^{-1}\times 273.15\,\text{K}}\times\left(1\,\text{cm}^3\,\text{g}^{-1} + 0.2\,\text{cm}^3\,\text{g}^{-1}\right)$$

$$\varphi = \frac{0.89\times10^{-3}\,\text{kg m}^{-1}\,\text{s}^{-1}\times 20000\,\text{g mol}^{-1}}{8.31441\,\text{kg m}^2\,\text{s}^{-2}\,\text{K}^{-1}\,\text{mol}^{-1}\times 273.15\,\text{K}}\times 1.2\times10^{-3}\,\text{m}^3\,\text{kg}^{-1} = 9.4\times10^{-9}\,\text{s} = 9.4\,\text{ns}$$

The fluorescence anisotropy observed for the receptor–ligand complex is:

$$\bar{r} = \frac{0.33}{1 + \dfrac{9\,\text{ns}}{9.4\,\text{ns}}} = 0.17$$

3.8 The regulation corresponds to competitive inhibition (cf. Figure 3.19).

3.9

(a) $\tau_{S_1}^{D,ET} = \left(k_{ET} + \tau_{S_1}^{D,0-1}\right)^{-1}$

$4\,\text{ns} = \left(k_{ET} + (10\,\text{ns})^{-1}\right)^{-1}$

$k_{ET} = 0.15\,\text{ns}^{-1}$

The rate of energy transfer is $k_{ET} = 0.15\,\text{ns}^{-1}$.

(b) $\Phi_{ET} = \dfrac{k_{ET}}{\tau_{S_1}^{D,0-1} + k_{ET}} = \dfrac{0.15\,\text{ns}^{-1}}{(10\,\text{ns})^{-1} + 0.15\,\text{ns}^{-1}} = 0.6$

The efficiency of energy transfer is $\Phi_{ET} = 0.6$.

(c) $\Phi_{ET} = \dfrac{{R_0}^6}{{R_0}^6 + r^6} = \dfrac{(2\,\text{nm})^6}{(2\,\text{nm})^6 + r^6} = 0.6$.

$64\,\text{nm}^6 = 0.6\times 64\,\text{nm}^6 + 0.6\times r^6$

$25.6\,\text{nm}^6 = 0.6\times r^6$

$r = \sqrt[6]{\dfrac{25.6}{0.6}}\,\text{nm} = 1.87\,\text{nm}$

The distance is $r = 1.87\,\text{nm}$.

3.10 The measurement of fluorescence polarization anisotropy, *r*, of a fluorescence dye attached to the smaller binding partner is the easiest and most robust method. However, if the smaller binding partner is so big that its rotational correlation time constant, ϕ, is comparable to or even larger than the fluorescence lifetime, τ_{S_1}, of the fluorescence marker then the observed anisotropy value is already close to its maximum and does not become significantly larger when binding to the large binding partner. As a consequence the dynamic sensitivity of the fluorescence polarization will be very limited. This size limitation is not relevant for a fluorescence lifetime binding assay. As with fluorescence polarization assays, the fluorescence lifetime can be measured in very short measuring times of less than a second and the read-out is very robust because the parameter does not depend on concentration or intensity fluctuations (ratiometric parameter). However, it is very hard to predict whether a distinct fluorescence marker changes its fluorescence lifetime due to the environmental changes in the case of a binding event. Therefore, the development of a lifetime assay can be quite time consuming and is based on trial and error. As for polarization assays, this is not so much the case when using Förster energy transfer to monitor the binding because the expected effects can be calculated using the equations given in the corresponding sections. The measurement of Förster energy transfer by comparison of the donor/acceptor fluorescence intensity or the donor fluorescence lifetime is also a ratiometric assay and thus very robust. However, the labelling chemistry is more demanding since, often, site-selective labelling is necessary and both binding partners have to be labelled. This also increases the risk of biasing the actual binding constant to be determined by the presence of the artificial labels.

Chapter 4

4.1 From a comparison with Figure 4.2 the following secondary structure element compositions can be estimated:

	Ellipticities			
Protein	~195 nm	~225 nm	~230 nm	Secondary structure elements
A	+	–	–	α-Helix
B	+	–	0	~⅓ α-Helix + ~⅔ β-sheet
C	+	0	+	β-Sheet
D	–	0	0	Random coil

4.2

$$\Phi(\lambda) = \frac{180 \times l \times \left(n_{\mathrm{l}}(\lambda) - n_{\mathrm{r}}(\lambda)\right)}{\lambda}$$

$$0.01 = \frac{180 \times 1\ \mathrm{cm} \times (n_{\mathrm{l}} - n_{\mathrm{r}})}{300\ \mathrm{nm}}$$

$$n_l - n_r = 1.7 \times 10^{-9}$$

$$n_l = n_r + 1.7 \times 10^{-9}$$

The speed of left circular polarized light:

$$c_{\mathrm{l}} = \frac{c_0}{n_{\mathrm{l}}} = \frac{c_0}{n_{\mathrm{r}} + 1.7 \times 10^{-9}}$$

The speed of right circular polarized light:

$$c_{\mathrm{r}} = \frac{c_0}{n_{\mathrm{r}}}$$

The speed difference:

$$c_{\mathrm{r}} - c_{\mathrm{l}} = \frac{c_0}{n_{\mathrm{r}}} - \frac{c_0}{n_{\mathrm{r}} + 1.7 \times 10^{-9}}$$

The refractive index of water is about 1.33. We assume $n_{\mathrm{r}} \approx 1.33$.

$$c_{\mathrm{r}} - c_{\mathrm{l}} = \frac{3 \times 10^8\ \mathrm{ms}^{-1}}{1.33} - \frac{3 \times 10^8\ \mathrm{ms}^{-1}}{1.33 + 1.7 \times 10^{-9}} = 0.29\ \mathrm{ms}^{-1}.$$

The difference in the speed of light for left- and right-handed circular polarized light is $c_{\mathrm{r}} - c_{\mathrm{l}} = 0.29\ \mathrm{ms}^{-1}$.

4.3 Comparison with Figure 4.6 shows that this corresponds to the case of scattering of light at molecules smaller than the optical wavelength.

Also, a comparison with Equation 4.14 provides the same result:

$$\frac{I_{\text{scat}}}{I_0} \propto \frac{8\alpha^2\pi^2}{\lambda^4 r^2}\left(1+\cos^2\theta\right)$$

In this case, $I_{\text{scat}} \propto \left(1+\cos^2\theta\right)$

$$\frac{I_{\text{scat}}^{90^\circ}}{I_{\text{scat}}^{180^\circ}} = \frac{1+\cos^2 90^\circ}{1+\cos^2 180^\circ} = \frac{1+0}{1+1} = 0.5$$

4.4 The dimension of the molecules can be estimated in the following way :

$V = M\left(\bar{v}+h\right)$ $\bar{v} \approx 1.0\ \text{cm}^3\ \text{g}^{-1}$, $h \approx 0.2\ \text{cm}^3\ \text{g}^{-1}$ (compare with Equation 3.23)

The volume of 100 kDa molecules per mole:

$$V = 100\ \text{kg mol}^{-1} \times \left(1\ \text{cm}^3\ \text{g}^{-1} + 0.2\ \text{cm}^3\ \text{g}^{-1}\right) = 1.2\times10^5\ \text{cm}^3\ \text{mol}^{-1}$$

If the molecules can be approximated as spheres the radius of one molecule can be estimated from its volume:

$$V = \frac{1.2\times10^5\ \text{cm}^3\ \text{mol}^{-1}}{6.02\times10^{23}\ \text{mol}^{-1}} = 2.0\times10^{-19}\ \text{cm}^3 = \tfrac{4}{3}\pi r^3.,\ r \text{ radius of the molecule:}$$

$r = 3.6\times10^{-7}\ \text{cm} = 3.6\ \text{nm}$

The radius of the 50kDa molecule is even smaller.

Therefore, the dimensions of all molecules are significantly smaller than the wavelength of the light and we can use

Rayleigh ratio $R_\theta = K \times c \times M$:

$$\frac{R_\theta^{100\ \text{kDa}}}{R_\theta^{50\ \text{kDa}}} = \frac{K\times c_{100\ \text{kDa}}\times M_{100\ \text{kDa}}}{K\times c_{50\ \text{kDa}}\times M_{50\ \text{kDa}}} = \frac{\frac{n' M_{100\ \text{kDa}}}{V'} M_{100\ \text{kDa}}}{\frac{n'' M_{50\ \text{kDa}}}{V''} M_{50\ \text{kDa}}} = \frac{cM_{100\ \text{kDa}}{}^2}{cM_{50\ \text{kDa}}{}^2} = \left(\frac{100\ \text{kDa}}{50\ \text{kDa}}\right)^2 = 4$$

The quotient of the Raleigh ratios $R_\theta^{100\ \text{kDa}} / R_\theta^{50\ \text{kDa}}$ is 4.

4.5 At $\theta = 0$, the optical path length will always be identical. With identical path lengths there will be no destructive interference. All other angles result in different optical path lengths that give rise to destructive interference effects.

4.6 Radius of gyration $R_G = 350$ nm

The maximum dimension of the biological object $l = 100$ nm

$$\frac{R_G}{l} = \frac{350\text{ nm}}{100\text{ nm}} = 3.5 \approx \sqrt{12} = 3.46$$

For long rods, $R_G = l_{rod}\sqrt{12}$. The object is rod-like.

4.7 From the secondary structure elements estimated in question 4.1 one can estimate, using Table 4.2, that the following Raman bands might show up:

Protein	Secondary structure elements	Raman band in Amide I (cm^{-1})
A	α-Helix	1640–1660
B	⅓ α-Helix + ~⅔ β-sheet	1640–1660, 1630–1640, weak band at 1680
C	β-Sheet	1630–1640, weak band at 1680
D	Random coil	1640–1650

However, because of different selection rules for Raman and absorption spectroscopy not all of these bands might show up.

Chapter 5

5.1 The energy difference between α-spin and β-spin is proportional to the magnetic field strength. The band width of an NMR line, however, remains more and less the same regardless of the magnetic field. As a consequence, bands that are close together in the spectrum can be better resolved when using a higher magnetic field strength.

5.2 NMR methods in which the absorption of continuous radio waves are measured take a very long measuring time since each NMR absorption wavelength has to be measured in turn. In pulsed NMR methods, the free induction decay observed after a 90°x radio wave pulse can be analyzed by Fourier transformation. The result of this procedure is one entire NMR spectrum in "one shot". This saves an enormous amount of measuring time. In addition, multi-dimensional NMR methods like COSY or NOESY are based on pulse sequences and allow us to obtain additional parameters like couplings between different nuclei. Without these advantages of pulsed NMR spectroscopy the analysis of biomolecule structure by NMR would be impossible.

5.3 The chemical shifts of the methylene group protons are influenced by the spins of the three neighbouring methyl protons. In the figure below the possible spins of these protons are illustrated along with the resulting line positions and intensities:

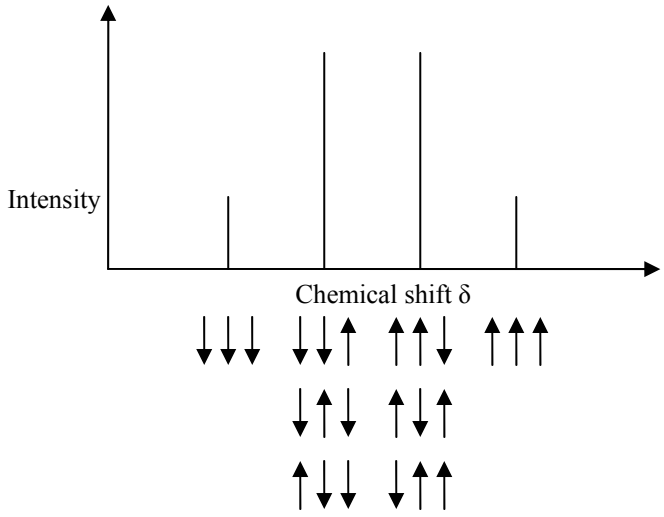

5.4 For this situation the magnetic moments of individual nuclei are preferentially in phase with an excess of either the α- or β spin population (see figure):

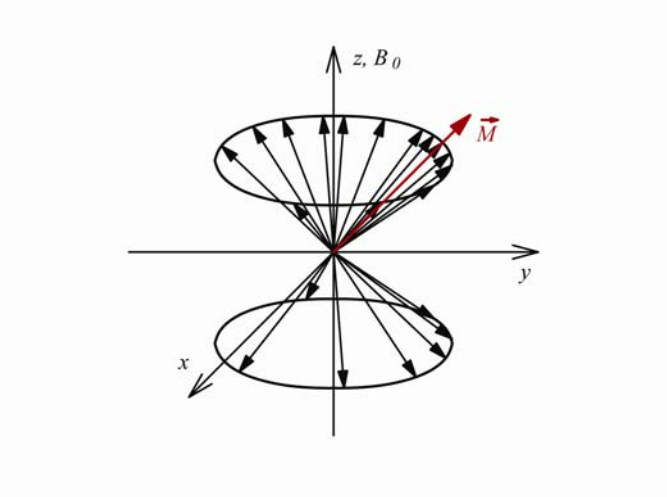

5.5 The trajectory in the laboratory frame corresponds to a helical-like movement of the total magnetization on a sphere and around the *z*-axis (see figure):

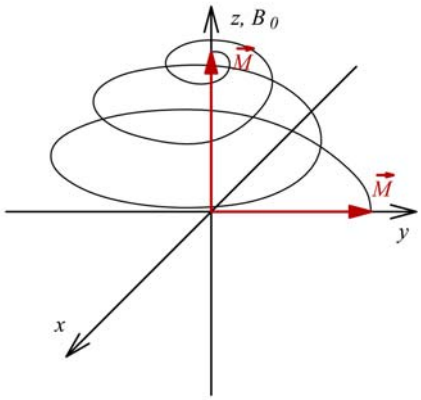

The figure represents only a schematic plot of the track of the magnetization vector. In reality there are several thousands of revolutions around the z-axis during a 90°x-pulse.

5.6

(a) This corresponds to a NOESY experiment (cf. Figures 5.13 and 5.14).

(b) After 1/8 of a full Larmor rotation the corresponding vector is pointing in the direction of the half diagonal of the *x*-*y* plane. The corresponding projections on the *x*- and *y*-axes are $\vec{M} \cdot \cos 45°$ or $\vec{M} / \sqrt{2} = 0.707\vec{M}$.

After the second 90°$_x$ pulse the corresponding projections are on the *z*- and *x*-axes. The component in the *x* direction disappears during t_m. Depending on the relaxation times T_1 and T_2 relative to t_m the component in the *z* direction remains and contributes to the FID after the third 90°$_x$ pulse.

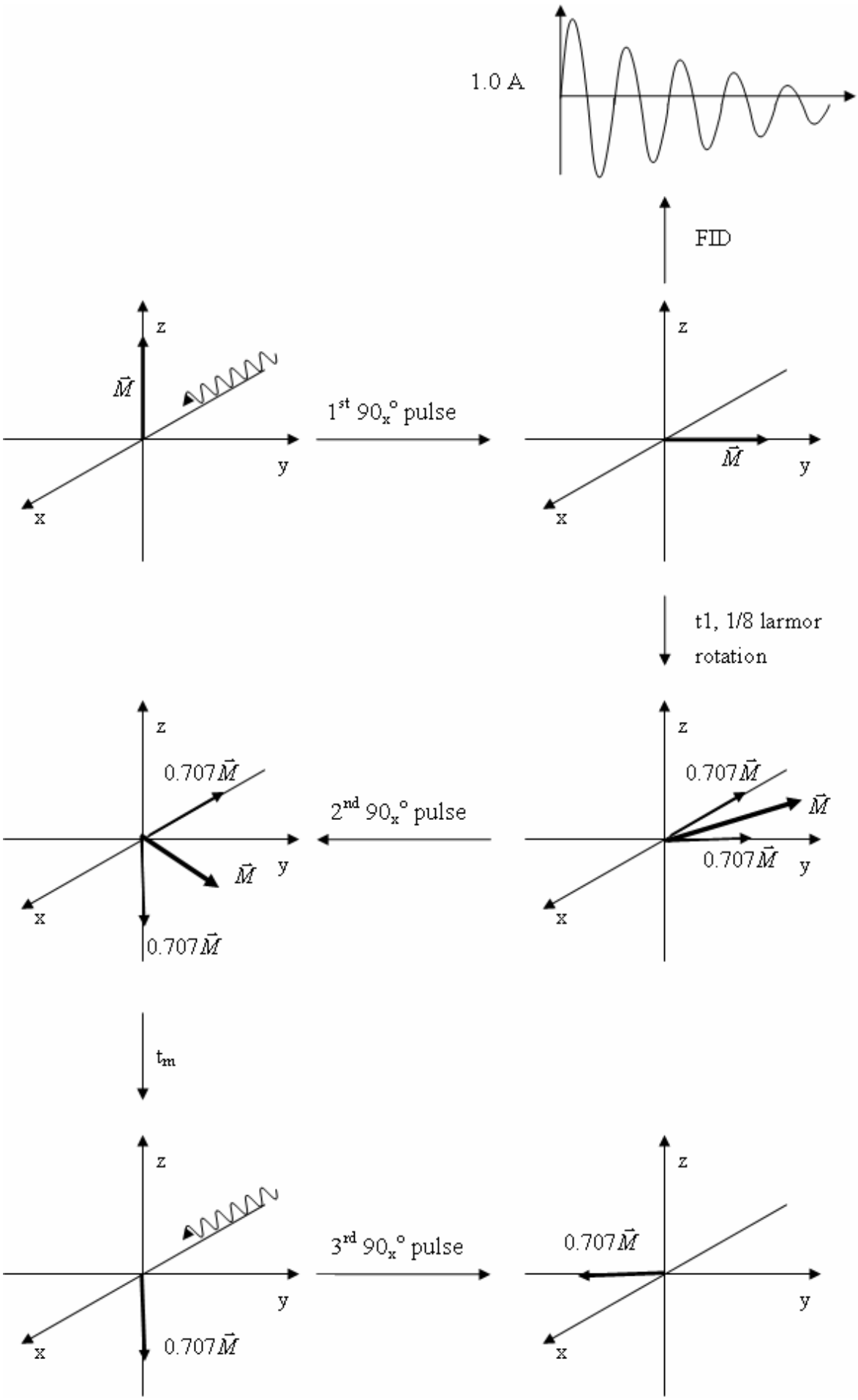
1.0 A
FID
z
$\vec{M}$
y
x
1st 90x° pulse
z
$\vec{M}$
y
x
t1, 1/8 larmor
rotation
z
0.707$\vec{M}$
$\vec{M}$
y
x
0.707$\vec{M}$
2nd 90x° pulse
z
0.707$\vec{M}$
$\vec{M}$
0.707$\vec{M}$
y
x
tm
z
y
x
0.707$\vec{M}$
3rd 90x° pulse
z
0.707$\vec{M}$
y
x

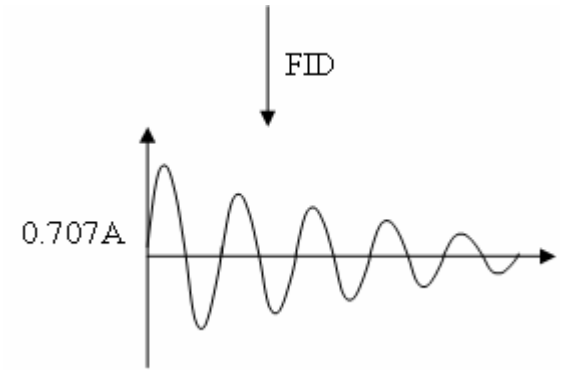

5.7 The nuclear Overhauser effect is a coupling between spin through space and can be effective up to 5 Å. When strong NOESY correlations are found between α-carbon hydrogens, H^{α} and hydrogens bound to nitrogens, H^{N}, of third amino acids further along in the primary sequence $H^{\alpha}(i)$-$H^{N}(i+3)$, then this clearly indicates the presence of an α-helix structure. These protons are very close in an α-helix structure because in the helix there are about 3.6 residues per turn.

5.8 From Figure 5.5 we can deduce that a scalar coupling of 8 Hz corresponds to a torsion angle Φ of around 100^{o}. Consequently, a β strand is the dominant structural element in the protein.

5.9 EPR absorption and emission wavelengths are in the microwave range. Because the generation of different wavelengths in the microwave range is technically difficult, an EPR spectrum is recorded by detecting the absorption or emission at a fixed microwave wavelength while simultaneously sweeping the magnetic field intensity.

5.10 The hyperfine coupling constant α depends on the orientation of the nitrogen p-orbital of the unpaired electron in TEMPO with respect to the external magnetic field. The orientation dependence of the hyperfine coupling constant gives rise to characteristic spectra for different rotational correlation times, φ.
The advantage of determining the rotational correlation time by EPR is the larger dynamic range of detectable rotational correlation times. Major drawbacks are the uncertainties in a quantitative determination of the rotational correlation time and longer acquisition time.

Chapter 6

6.1 Because of the continuous sample flow and ion generation, TOF analysis can not be directly used for the determination of *m*/*z* after ESI. Normally, quadrupole mass spectrometers and ion traps are used to connect with ESI. However, it is also possible to perform TOF analysis in combination with ESI to detect in a pulsed manner ions in the direction perpendicular to the continuous ion flow.

6.2

(a)

$$\frac{m}{z} = \frac{2eU}{L^2} t^2$$

$$\frac{m}{z} = \frac{2 \times e \times 5\ \text{kV}}{(2m)^2} \times (250\ \mu\text{s})^2 = \frac{1 \times 10^4\ \text{eV}}{4m^2} \times 62500 \times 10^{-12}\ \text{s}^2$$

$$\frac{m}{z} = 2.5 \times 10^{-20}\ \text{g}$$

$$1\ \text{eV} = 1.6 \times 10^{-19}\ \text{J}$$

$$1\ \text{J} = 1\ \text{kg m}^2\ \text{s}^{-2}$$

For MALDI, in many cases unharmed biomolecules with only one or a few charges are created. Consequently, we can assume that *z* equals to1:

$$m = 2.5 \times 10^{-20}\ \text{g}$$

$$M = 2.5 \times 10^{-20}\ \text{g} \times 6.02 \times 10^{23}\ \text{mol}^{-1} = 15050\ \text{gmol}^{-1} = 15\ \text{kDa}$$

The molecular mass of the molecule is M = 15 kDa. Since the molecular weight of one amino acid is on average about 100 Da, 15 kDa = 15000 Da corresponds to about 136 amino acids. Since a biomolecule is usually only called peptide if it contains less than 100 amino acids the molecule can be called a quite small protein.

(b)

$$m = \frac{100\ \text{gmol}^{-1}}{6.02 \times 10^{23}\ \text{mol}^{-1}} = 1.66 \times 10^{-22}\ \text{g}$$

We assume again that only molecules with one charge are created:

$$\frac{m}{z} = 1.66 \times 10^{-22}\ \text{g} = \frac{2 \times e \times 5\ \text{kV}}{(2m)^2} t^2$$

$$t^2 = \frac{1.66 \times 10^{-22}\ \text{g} \times 4m^2}{1 \times 10^4\ \text{eV}} = 4.15 \times 10^{-10}\ \text{s}^2$$

$$t = 2 \times 10^{-5}\ \text{s} = 20\ \mu\text{s}$$

The ions of the fluorescent label will be detected 20 µs after the laser irradiation.

6.3 According to Table 6.1, 2,5-dihydroxybenzoic acid is suitable for the analysis of peptides as well as oligonucleotides.

6.4 In a single 1 kDa peptide there are $(1000\ \text{gmol}^{-1} \times 80\%) / 12.0107\ \text{gmol}^{-1} = 66.6 \approx 67$ carbon atoms. The probabilities for the different isotopomers in this case are:

^{13}C atom	^{12}C atom	Probability	Normalization
0	67	$0.9889^{67} = 0.4734$	1
1	66	$\binom{67}{1} \times 0.0111 \times 0.9889^{66} = 0.3560$	0.752
2	65	$\binom{67}{2} \times 0.0111^{2} \times 0.9889^{65} = 0.1319$	0.279
3	64	$\binom{67}{3} \times 0.0111^{3} \times 0.9889^{64} = 0.0321$	0.068
4	63	$\binom{67}{4} \times 0.0111 \times 0.9889^{63} = 0.0058$	0.012
5	62	$\binom{67}{5} \times 0.0111^{5} \times 0.9889^{62} = 0.0058$	0.002

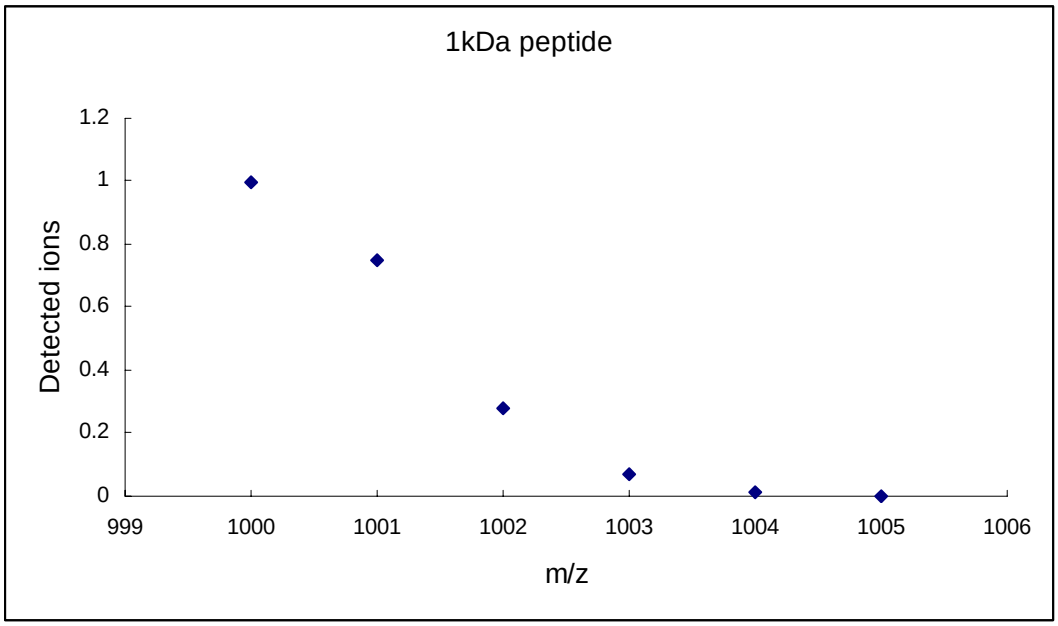

In a single 10 kDa protein there are $(10000\ \text{gmol}^{-1} \times 80\%) / 12.0107\ \text{gmol}^{-1} = 666.07 \approx 666$ carbon atoms . The probabilities for the different isotopomers in this case are:

^{13}C atom	^{12}C atom	Probability	Normalization
0	666	$0.9889^{666} = 0.0006$	0.004
1	665	$C_1^{666} 0.0111 \times 0.9889^{665} = 0.0044$	0.030
2	664	$C_2^{666} 0.0111^2 \times 0.9889^{664} = 0.0165$	0.111
3	663	$C_3^{666} 0.0111^3 \times 0.9889^{663} = 0.0401$	0.277
4	662	$C_4^{666} 0.0111^4 \times 0.9889^{662} = 0.0762$	0.514
5	661	$C_5^{666} 0.0111^5 \times 0.9889^{661} = 0.1132$	0.764
6	660	$C_6^{666} 0.0111^6 \times 0.9889^{660} = 0.1400$	0.945
7	659	$C_7^{666} 0.0111^7 \times 0.9889^{659} = 0.1482$	1.000
8	658	$C_8^{666} 0.0111^8 \times 0.9889^{658} = 0.1370$	0.925
9	657	$C_9^{666} 0.0111^9 \times 0.9889^{657} = 0.1124$	0.759
10	656	$C_{10}^{666} 0.0111^{10} \times 0.9889^{656} = 0.0829$	0.560
11	655	$C_{11}^{666} 0.0111^{11} \times 0.9889^{655} = 0.0555$	0.375
12	654	$C_{12}^{666} 0.0111^{12} \times 0.9889^{654} = 0.0340$	0.229
13	653	$C_{13}^{666} 0.0111^{13} \times 0.9889^{653} = 0.0192$	0.130
14	652	$C_{14}^{666} 0.0111^{14} \times 0.9889^{652} = 0.0101$	0.068
15	651	$C_{15}^{666} 0.0111^{15} \times 0.9889^{651} = 0.0049$	0.033
16	650	$C_{16}^{666} 0.0111^{16} \times 0.9889^{650} = 0.0022$	0.015

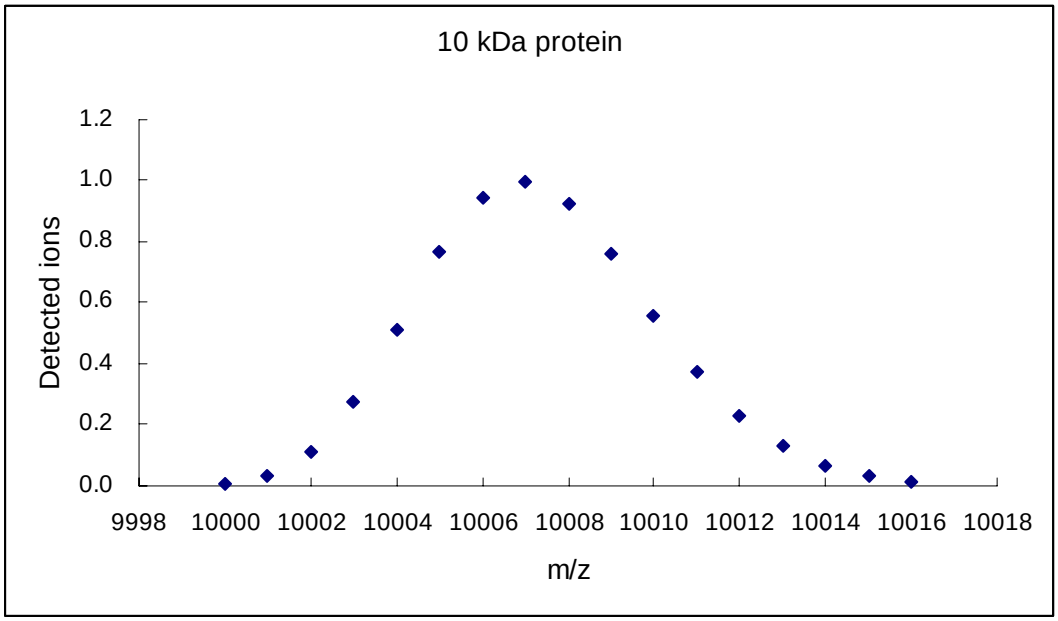

6.5 By looking at Figure 6.11 we see that this can be achieved by decreasing the ratio a/q.
Since $a/q = 2U/V$ this can be achieved by decreasing the constant voltage U or increasing the maximum amplitude of the oscillating voltage V.

6.6 This is especially useful, for example, if only a very small amount of the sample of interest is available in a solution that has to be first separated by HPLC. Then the all ions of a certain mass-to-charge ratio originating from this sample can be analysed one after another. If a quadrupole mass analyzer is used many ions are discarded. A TOF also allows analysis of all ions but it is more demanding to use for the analysis of continuously generated ions eluted from HPLC.

6.7 The corresponding mass spectrum would ideally look as follows:

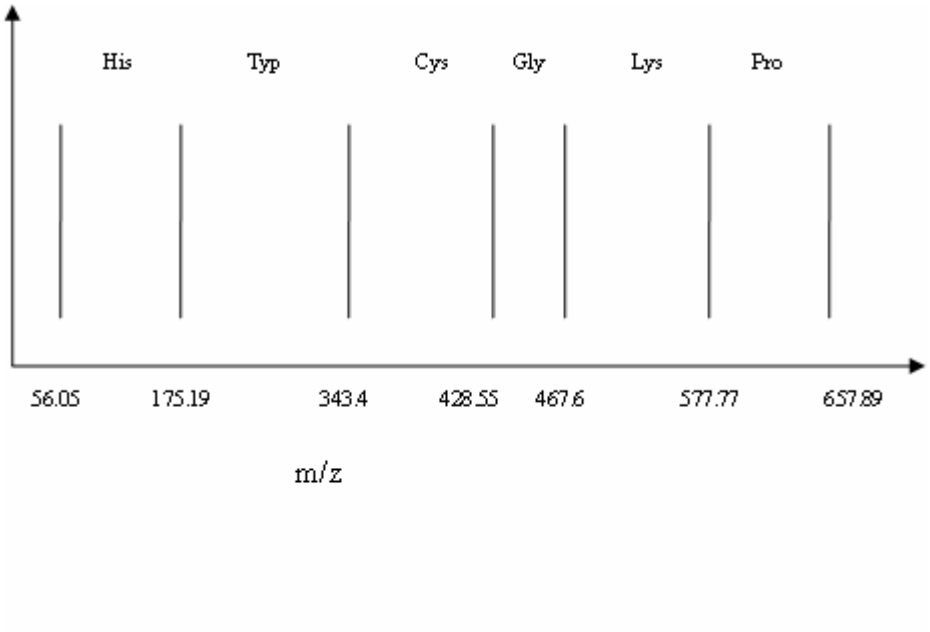

6.8 Using the collisions of the ions with an inert gas in MS-MS or MSn techniques allows us to purposely fragment the tetra- or trimer. It will then be possible under appropriate experimental conditions to identify masses that correspond either to a quarter or one-third of the entire protein-multimer. Depending on the result the original complex can then be assigned as either a tetra- or trimer.

Chapter 7

7.1 The back aperture of the microscope objective should be completely illuminated to achieve a small r_0 because then the narrowest diffraction limited focus is generated according to Equation 7.1 (cf. Figure 7.2). The value of z_0 is predominantly controlled by the alignment of the pinhole (cf. Figure 7.4). In addition the use of microscope optics of very high quality is necessary to achieve the best resolution of the dimensions z_0 and r_0.

7.2 The diffraction limited resolution at different numerical apertures and wavelengths can be calculated according to Abbe's law (Equation 7.1):

$x \approx \frac{\lambda}{2 \cdot n \cdot \sin\varphi}$ with $n \cdot \sin\varphi$ being the numerical aperture.

The corresponding resolutions are summarized in the following table:

		Wavelength(nm)		
		400	600	800
Numerical aperture	1.0	200	300	400
	1.2	167	250	333
	1.33	150	226	300

$1.33 \times \sin\varphi = 1.0$

$\sin\varphi = 0.75$

$\varphi = \sin^{-1} 0.75 = 48.7^{\circ}$

The collection efficiency can be calculated according to:

$\frac{1 - \cos\varphi}{2} = 0.17$

The collection efficiency for the different numerical apertures is therefore:

Numerical aperture	φ (°)	Collection efficiency
1.0	48.7	0.17
1.2	64.5	0.28
1.33	90	0.5

7.3 The following figure first illustrates the focus for a collimated beam that is perpendicular to the lens:

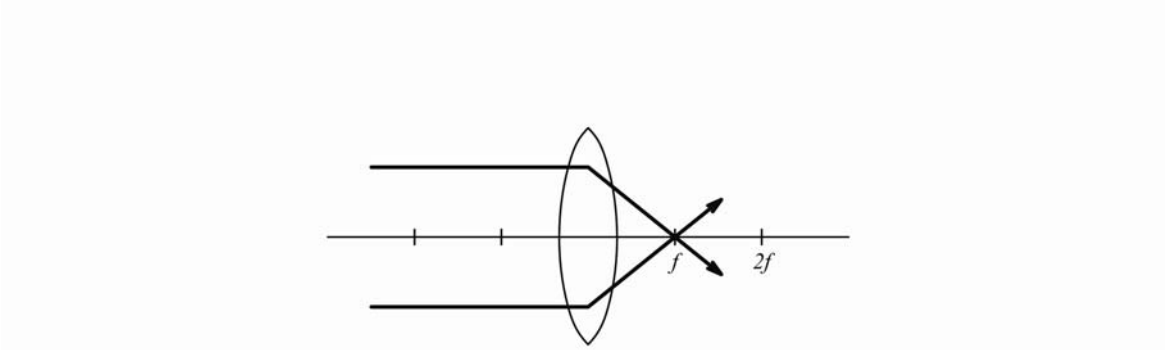

A collimated beam that is not perpendicular to the lens results in a lateral shift of the focus:

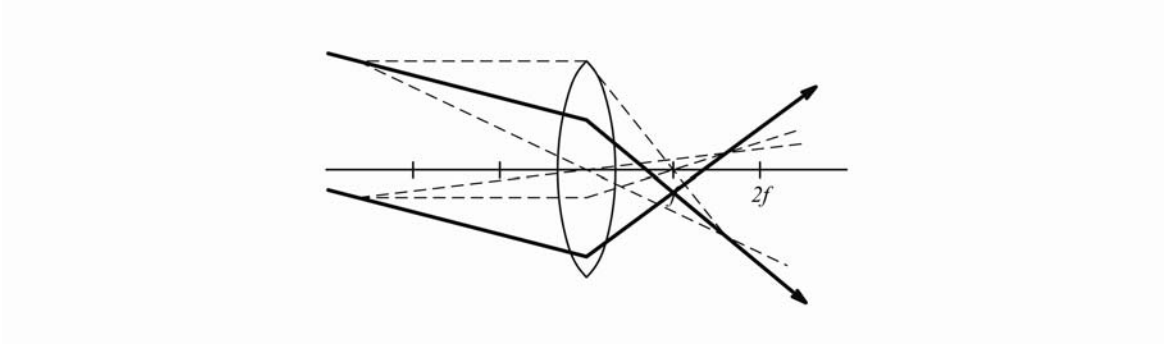

A slightly focused beam results in a shift of the focus closer to the lens:

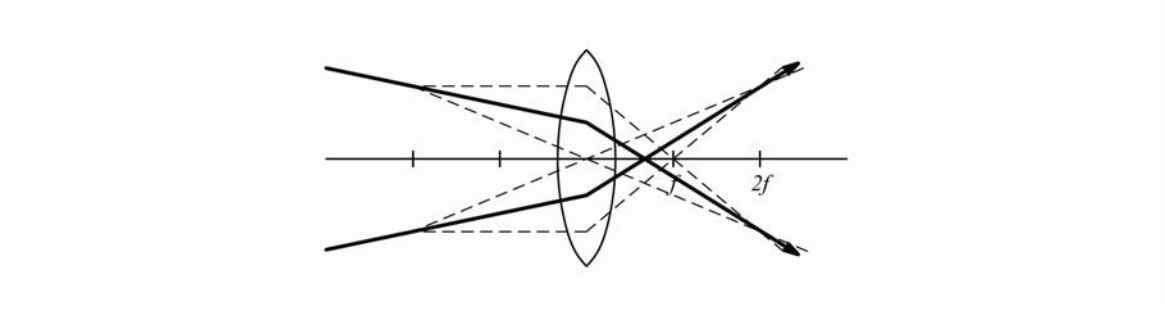

A slightly divergent beam results in a shift of the focus away from the lens:

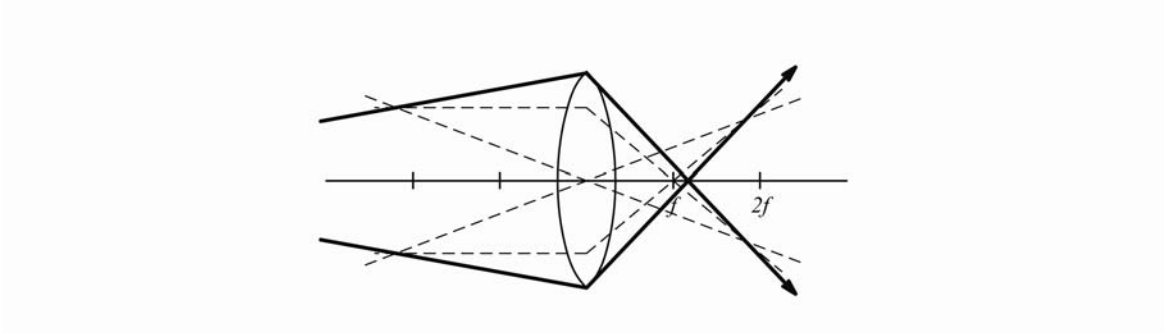

There is no principle difference in the optical paths of light being focused to a certain spot of and fluorescence light being emitted from that spot being collected by the objective. This is true for all four cases.

7.4 When the object is positioned in the focal plane a slightly focused excitation beam illuminates a larger area of this object (see area in the figure indicated by a wavy line).

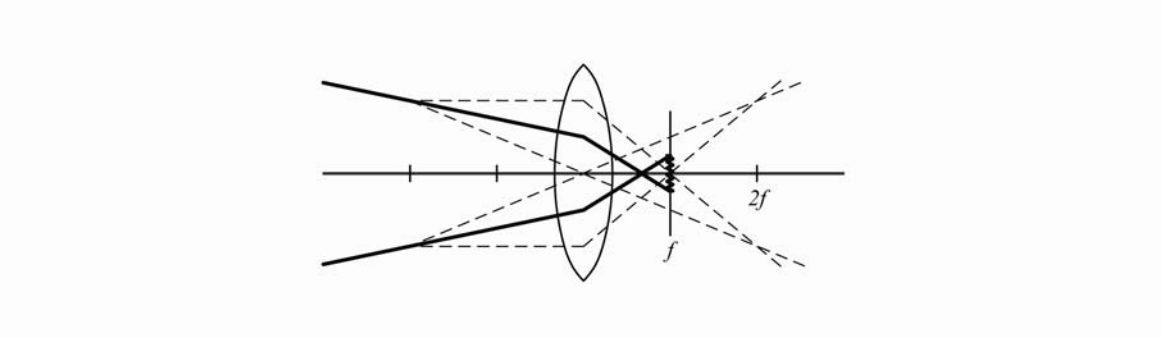

7.5

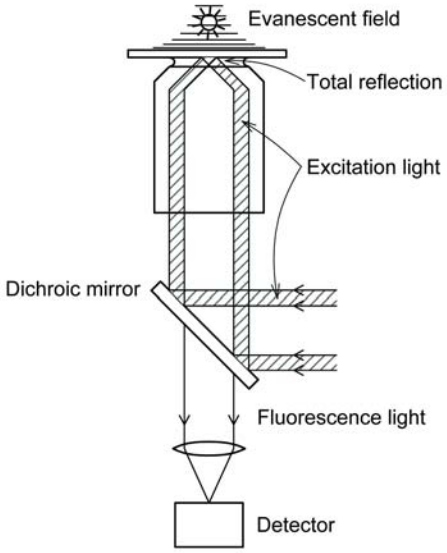

7.6 Since for a distinct vibronic transition, $S_0^{v''=0} \leftrightarrow S_1^{v'=x}$, the probability that a photon stimulates an induced emission, $S_1^{v'=x} \rightarrow S_0^{v''=0}$, is exactly the same as the probability that a photon is absorbed, $S_0^{v''=0} \rightarrow S_1^{v'=x}$, a STED beam of high intensity and of the same wavelength as the PUMP beam at most populates both states, $S_0^{v''=0}$ and $S_1^{v'=x}$, equally. The STED beam will always populate $S_1^{v'=x}$ by absorption. However, usually, quick vibrational relaxation, $S_1^{v'=x} \rightsquigarrow S_1^{v'=0}$, on the ps-time scale will occur with the overall result that many molecules remain excited for longer periods in $S_1^{v'=0}$ on a ns-time scale, corresponding to the lifetime τ_{S_1}. If , however, the STED beam wavelength is tuned to a wavelength corresponding to a transition $S_1^{v'=0} \leftrightarrow S_0^{v''=y}$ then only induced emission $S_1^{v'=0} \rightarrow S_0^{v''=y}$ can occur. This is because at room temperature, usually, all remaining molecules in the electronic ground state are in the vibrational state $S_0^{v''=0}$ and not $S_0^{v''=y}$. As a consequence no corresponding absorption, $S_0^{v''=y} \rightarrow S_1^{v'=0}$, by STED photons is possible and the excited state $S_1^{v'=0}$ can be almost entirely depleted by the STED beam if the intensity is high enough. That this situation remains even

after an induced emission, $S_1^{v'=0} \rightarrow S_0^{v''=y}$, requires very rapid depopulation of $S_0^{v''=y}$ by the vibrational relaxation $S_0^{v''=y} \rightsquigarrow S_0^{v''=0}$.

7.7 From a single fluorescent protein or fluorescence marker only a limited number of photons can be detected per time unit. Photo-bleaching potentially further reduces the total number of detectable photons. As a consequence, the Gaussian like fluorescence peak for which the centre has to be determined as exactly as possible can only be imaged with an accuracy limited by photon shot noise. Inaccuracies of fitting a two-dimensional Gaussian function to the noisy fluorescence peak is one of the most important factors limiting the resolution in PALM microscopy.

Chapter 8

8.1 For the optical detection of single molecules

(a) A small observation volume is necessary to reduce background luminescence from the solvent environment.

(b) A small concentration of the fluorescing particles is necessary to observe at most one particle in that volume.

(c) A high fluorescence quantum yield of the fluorescence particle is necessary for a high signal-to-noise ratio.

(d) A large numerical aperture of the microscope objective helps to collect as many fluorescence photons as possible from a single fluorescence marker.

(e) Only little losses of fluorescence at the further optical components such as filters, lenses, mirrors and dichroic mirrors are desirable.

(f) Finally, a high photon detection efficiency and a low background noise of the detector is necessary.

The detection of single biomolecules is especially advantageous, for example, when important intermediate steps of biomolecular processes cannot be measured in the ensemble. This is very often the case because they do not occur simultaneously but rather at arbitrary times that cannot be controlled externally.

8.2 One possibility is to label, for example, α-subunit and the β-subunit site selectively with a donor and acceptor fluorescence marker. Such site selective labelling can be achieved by point-mutation of the DNA of these subunits corresponding to insertion or deletion of cysteine residues. The sites should be chosen in a way that the donor and acceptor fluorescence dyes come close together only during the passing of the labelled α-subunits by the β-subunit without hindering the rotation. The corresponding subunits can then be expressed by expression organisms and be labelled by using thiol reactive fluorescence markers. In the assembly to complexes immobilized on a surface, as shown in Figure 8.4, one could use concentrations of the labelled α-subunits and unlabelled α-subunits that result statistically in complexes that either contain just one or no labelled α-subunits. The complexes carrying a labelled α-subunits can easily be identified by the photon wavelengths corresponding to the label. Then the efficiency of Förster energy transfer can be monitored on a single-molecule basis as a function of, for example, ATP concentration.

8.3 The detected positions of the fluorescence marker should be equidistant because the labelled "foot" of one myosin dimer steps always in front of or behind the other by the same step-size (compare with the figure below).

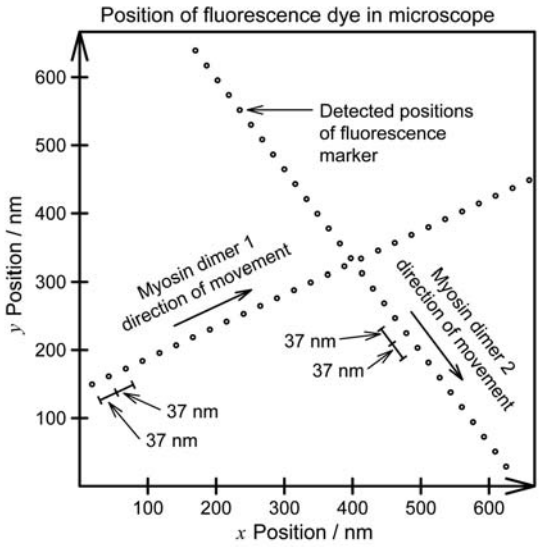

8.4 (a) To calculate the average number of fluorescing proteins, fragments or dyes in the focus and the corresponding macroscopic concentration we can use the following formulas.

$$G(\sim 0) = \frac{1}{\langle C \rangle V_{\text{eff}}} = \frac{1}{\langle N \rangle}$$

$$\langle N \rangle = \frac{1}{G(\sim 0)}$$

$$\langle C \rangle = \frac{\langle N \rangle}{V_{\text{eff}}}$$

$$V_{\text{eff}} = \pi^{\frac{3}{2}} r_0^2 z_0 = \pi^{\frac{3}{2}} (0.2\ \mu\text{m})^2 (1\ \mu\text{m}) = 2.2 \times 10^{-19}\ \text{m}^3$$

The corresponding results are summarized in the table below:

	Correlation amplitude	$\langle I_{\text{Fl}}(t) \rangle$ (s^{-1})	$\langle N \rangle$	$\langle C \rangle$ (nM)
Fluorescently labelled protein	6	100000	0.167	1.26
Protein digested by thrombin	2	100000	0.5	3.78
Protein digested by subtilisin	1	100000	1	7.55
Free fluorescent label	1	100000	1	7.55

(b) & (c)

To determine the average number of labels bound per protein we can calculate the particle brightness, $I_{\mathrm{Fl}}^{\mathrm{Particle}} = \langle I_{\mathrm{Fl}}(t) \rangle / \langle N \rangle$, and divide the corresponding number by the brightness observed for a single free fluorescent label. The corresponding results are given in the table below:

	$\langle N \rangle$	$\langle I_{\mathrm{Fl}}(t) \rangle$ (s^{-1})	Particle brightness (s^{-1})	Labels per protein or fragment that still carries fluorescence labels
Fluorescently labelled protein	0.167	100000	600000	6
Protein digested by thrombin	0.5	100000	200000	2
Protein digested by subtilisin	1	100000	100000	1
Free fluorescent label	1	100000	100000	1

In the sample digested by subtilisin the original protein of 60 kDa molecular weight is digested into fragments of ~6 kDa. That means that one protein resulted on average in ~10 fragments. However, the observed number of fluorescing particles increases only by a factor of 6 during the digestion. From the particle brightness we know that the fragments that still carry a fluorescence markers carry on average only one fluorescence label. Therefore we have on average only 6 fragments out of the 10 fragments per original protein that carry a single fluorescence label. The percentage of protein fragments in the sample digested by subtilisin that still carries a fluorescence label is ~60 %.

(d) The molecular weight of the undigested fluorescently labelled protein is
$60\ \mathrm{kDa} + 6 \times 0.4\ \mathrm{kDa} = 62.4\ \mathrm{kDa}$

We first estimate its volume by using $V = M(\bar{v} + h)$ and calculate the radius that would correspond to a sphere:

$$V = \frac{62.4\ \mathrm{kg\ mol^{-1}} \times \left(1.0\ \mathrm{cm^3\ g^{-1}} + 0.2\ \mathrm{cm^3\ g^{-1}}\right)}{6.02 \times 10^{23}\ \mathrm{mol^{-1}}} = 1.24 \times 10^{-19}\ \mathrm{cm^3}$$

$$V = \tfrac{4}{3}\pi r_{\mathrm{p}}^{\,3} = 1.24 \times 10^{-19}\ \mathrm{cm^3}$$

$$r_{\mathrm{p}} = 3.1\ \mathrm{nm}$$

From the radius we can estimate the diffusion coefficient:

$$D = \frac{kT}{6\pi r_{\mathrm{p}} \eta} = \frac{1.38055 \times 10^{-23}\ \mathrm{J\ K^{-1}} \times 300\ \mathrm{K}}{6 \times 3.14 \times 3.1\ \mathrm{nm} \times 0.89 \times 10^{-3}\ \mathrm{kg\ m^{-1}\ s^{-1}}} = 8.0 \times 10^{-11}\ \mathrm{m^2\ s^{-1}}$$

Finally, we can calculate the diffusional time constant using the diffusion coefficient:

$$\tau_{\mathrm{D}} = \frac{r_0^{\,2}}{4D} = \frac{\left(0.2\ \mathrm{nm}\right)^2}{4 \times 8.0 \times 10^{-11}\ \mathrm{m^2\ s^{-1}}} = 125\ \mu\mathrm{s}$$

The same estimate for the free fluorescent label is shown below:

$$V = \frac{0.4\ \text{kg mol}^{-1} \times \left(1.0\ \text{cm}^3\ \text{g}^{-1} + 0.2\ \text{cm}^3\ \text{g}^{-1}\right)}{6.02 \times 10^{23}\ \text{mol}^{-1}} = 8.0 \times 10^{-22}\ \text{cm}^3$$

$$V = \tfrac{4}{3}\pi r_\text{p}^{\,3} = 8.0 \times 10^{-22}\ \text{cm}^3$$

$$r_\text{p} = 0.57\ \text{nm}$$

$$D = \frac{kT}{6\pi r_\text{p}\eta} = \frac{1.38055 \times 10^{-23}\ \text{J K}^{-1} \times 300\ \text{K}}{6 \times 3.14 \times 0.57\ \text{nm} \times 0.89 \times 10^{-3}\ \text{kg m}^{-1}\ \text{s}^{-1}} = 4.3 \times 10^{-10}\ \text{m}^2\ \text{s}^{-1}$$

$$\tau_\text{D} = \frac{r_0^{\,2}}{4D} = \frac{\left(0.2\ \text{nm}\right)^2}{4 \times 4.3 \times 10^{-10}\ \text{m}^2\ \text{s}^{-1}} = 23\ \mu\text{s}$$

(e) The autocorrelation amplitude can be calculated using:

$$G_\text{Di}\left(\tau\right) = \frac{1}{\left\langle N \right\rangle} \cdot \frac{1}{1 + \dfrac{\tau}{\tau_\text{D}}} \cdot \frac{1}{\sqrt{1 + \left(\dfrac{r_0}{z_0}\right)^2 \dfrac{\tau}{\tau_\text{D}}}}$$

The result for the undigested fluorescently labelled protein is:

$$G_\text{Di}\left(100\ \mu\text{s}\right) = \frac{1}{0.167} \cdot \frac{1}{1 + \dfrac{100\ \mu\text{s}}{125\ \mu\text{s}}} \cdot \frac{1}{\sqrt{1 + \left(\dfrac{0.2\ \mu\text{m}}{1\ \mu\text{m}}\right)^2 \dfrac{100\ \mu\text{s}}{125\ \mu\text{s}}}} = 3.3$$

The corresponding result for the free fluorescent label is:

$$G_\text{Di}\left(100\ \mu\text{s}\right) = \frac{1}{1} \cdot \frac{1}{1 + \dfrac{100\ \mu\text{s}}{23\ \mu\text{s}}} \cdot \frac{1}{\sqrt{1 + \left(\dfrac{0.2\ \mu\text{m}}{1\ \mu\text{m}}\right)^2 \dfrac{100\ \mu\text{s}}{23\ \mu\text{s}}}} = 0.17$$

(f) To calculate the average number of photons detected per transit we simply multiply the particle brightness $\left\langle I_\text{Fl}\left(t\right)\right\rangle$ by the diffusional time τ_D. The result for the undigested fluorescently labelled protein is:

$$600000\ \text{s}^{-1} \times 125\ \mu\text{s} = 75$$

and for the free fluorescent label:

$$100000\ \text{s}^{-1} \times 23\ \mu\text{s} = 2.3$$

(g) The maximum anisotropy for molecules having a non-collinear transition dipole moments is:

$$r_0 = 0.4 \times \left(\frac{3\cos^2 \alpha - 1}{2} \right)$$

Since $\alpha = 0°$ the value for the fluorescent label is $r_0 = 0.4$.

We can estimate the rotational correlation time for the undigested fluorescently labelled protein by using:

$$\varphi = \frac{\eta V}{RT} = \frac{\eta M}{RT}\left(\bar{v} + h\right) = \frac{0.89 \times 10^{-3}\ \text{kg m}^{-1}\ \text{s}^{-1} \times 62.4\ \text{kg mol}^{-1}}{8.314\ \text{J K}^{-1}\ \text{mol}^{-1} \times 300\ \text{K}}\left(1.0\ \text{cm}^3\ \text{g}^{-1} + 0.2\ \text{cm}^3\ \text{g}^{-1}\right)$$

$$\varphi = 2.67 \times 10^{-8}\ \text{s} = 26.7\ \text{ns}$$

The corresponding average fluorescence anisotropy is:

$$\bar{r} = \frac{r_0}{1 + \frac{\tau_{s_1}}{\varphi}} = \frac{0.4}{1 + \frac{4\ \text{ns}}{26.7\ \text{ns}}} = 0.35$$

Analogously, the average fluorescence anisotropy for the free fluorescent label is:

$$\varphi = \frac{\eta V}{RT} = \frac{\eta M}{RT}\left(\bar{v} + h\right) = \frac{0.89 \times 10^{-3}\ \text{kg m}^{-1}\ \text{s}^{-1} \times 0.4\ \text{kg mol}^{-1}}{8.314\ \text{J K}^{-1}\ \text{mol}^{-1} \times 300\ \text{K}}\left(1.0\ \text{cm}^3\ \text{g}^{-1} + 0.2\ \text{cm}^3\ \text{g}^{-1}\right)$$

$$\varphi = 1.71 \times 10^{-10}\ \text{s} = 0.17\ \text{ns}$$

$$\bar{r} = \frac{r_0}{1 + \frac{\tau_{s_1}}{\varphi}} = \frac{0.4}{1 + \frac{4\ \text{ns}}{0.17\ \text{ns}}} = 0.016$$

The sum of the average number of photons detected by the parallel and perpendicular detector during single transits, $I_{\parallel} + I_{\perp}$, must correspond to the number of photons per single transits calculated in the previous question:

$I_{\parallel} + I_{\perp} =$ photons per molecular transit.

In addition they are related to the anisotropy by:

$$\bar{r} = \frac{I_{\parallel} - I_{\perp}}{I_{\parallel} + 2I_{\perp}}$$

which gives:

$$\frac{I_{\parallel}}{I_{\perp}} = \frac{2\bar{r}+1}{1-\bar{r}}$$

For the intensities detected in the detectors for parallel and vertical polarized light we know that:

$$I_{\parallel} = (2\bar{r}+1)k\,,\; I_{\perp} = (1-\bar{r})k$$

with *k* being a proportionality constant.

With the number of photons per molecular transit:

$$I_{\parallel} + I_{\perp} = (\bar{r}+2)k$$

we can calculate absolute values for the photons detected with the detectors for parallel and vertical polarized light.
The values are summarized in the following table:

	Photons per transit	$\bar{r}$	$\frac{I_{\parallel}}{I_{\perp}}$	$I_{\parallel}$	$I_{\perp}$
Fluorescently labelled protein	75	0.35	2.62	54.3	20.7
Free fluorescent label	2.3	0.016	1.05	1.18	1.12

8.5 The triplet state fraction can be calculated from $G_T = 0.3, \frac{1}{\langle N \rangle} = 0.6$ using the following formula:

$$T = \frac{G_T \cdot \langle N \rangle}{1 + G_T \cdot \langle N \rangle}$$

The result is $T = \frac{G_T \cdot \langle N \rangle}{1 + G_T \cdot \langle N \rangle} = \frac{G_T}{\frac{1}{\langle N \rangle} + G_T} = \frac{0.3}{0.6 + 0.3} = 0.33$.

8.6 Dual colour fluorescence cross-correlation spectroscopy is more advantageous when both binding partners are large biomolecules, for example, an antibody and a large protein–antigen. In this case the dynamic range of fluorescence polarization does not suffice because the rotational diffusion of both binding partners is larger than the fluorescence lifetime of fluorescence markers. Cross-correlation still provides very robust information about binding regardless of the size of the binding partners.

8.7 The Dichroic mirror in a dual colour confocal microscope set-up must reflect both excitation wavelengths but must let pass simultaneously the major part of both fluorescence

wavelengths (see figure below). Of course the filters for the two fluorescence markers' wavelengths must also fit with the corresponding fluorescence spectra.

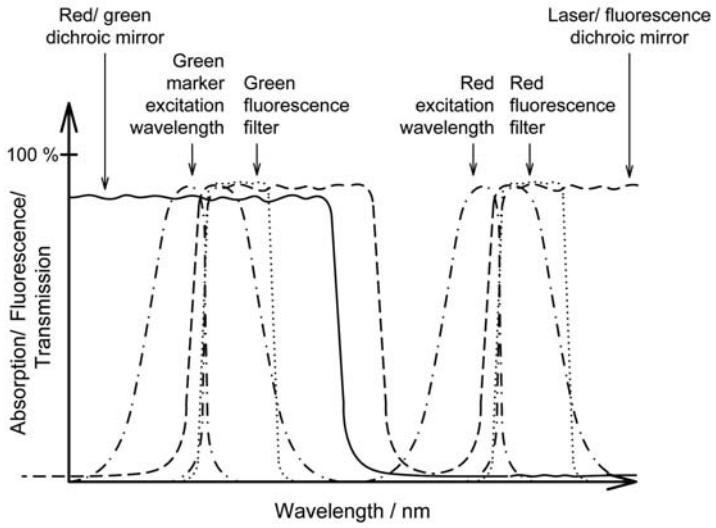

8.8 The particle numbers of the ligand, receptor and receptor–ligand complex can be calculated from the correlation amplitudes:

$$G_{\mathrm{R}}(0) = 0.5,\ G_{\mathrm{G}}(0) = 1,\ G_{\mathrm{RG}}(0) = 0.3$$

$$\langle N \rangle = \frac{1}{G(0)}$$

$$\langle N_{\mathrm{R}} \rangle = \frac{1}{0.5} = 2,\ \langle N_{\mathrm{G}} \rangle = \frac{1}{1} = 1,\ \langle N_{\mathrm{RG}} \rangle = \frac{0.3}{0.5 \times 1} = 0.6$$

$$V_{\mathrm{eff}} = \pi^{\frac{3}{2}} r_0^2 z_0 = 2.2 \times 10^{-16}\ \mathrm{L}$$

For the reaction scheme:

G-receptor + ligand-R → G-receptor–ligand-R

the dissociation constant is defined as:

$$K = \frac{C_{\text{G-receptor}} \cdot C_{\text{ligand'-R}}}{C_{\text{G-receptorligand-R}}}.$$

Calculating the concentrations from the detection volume and particle numbers results in the following dissociation constant:

$$K = \frac{\frac{2}{N_A \times V_{eff}} \times \frac{1}{N_A \times V_{eff}}}{\frac{0.6}{N_A \times V_{eff}}} = \frac{3.33}{N_A V_{eff}}$$

$$K = \frac{3.33}{6.02 \times 10^{23}\ \text{mol}^{-1} \times 2.2 \times 10^{-16}\ \text{L}} = 2.5 \times 10^{-8}\ \text{M}$$

8.9 By a total reflection the absolute momentum changes for a single photon as follows:

$$p = \frac{h}{\lambda}$$

$$\left|\Delta\vec{p}\right| = \left|\vec{p}_A - \vec{p}_B\right| = 2p = \frac{2h}{\lambda}$$

The resulting force of 100 W photons is then:

$$\left|\vec{F}\right| = \left|\frac{dN \cdot \Delta\vec{p}}{dt}\right| = \cdot\frac{P}{h\nu} \cdot \frac{2h}{\lambda} = \frac{P\lambda}{hc} \cdot \frac{2h}{\lambda} = \frac{2P}{c} = \frac{2 \cdot 100 Js^{-1}}{3 \cdot 10^8 ms^{-1}} = 6.7 \cdot 10^{-6} N$$

$$\left(P = \frac{dN}{dt} \cdot h\nu\right)$$

8.10 The force of a laminar flow on a sphere is:

$$F_{\text{laminar}} = 6\pi\eta r v = 6\pi \times 0.89 \times 10^{-3}\ \text{kg m}^{-1}\ \text{s}^{-1} \times 0.5\ \mu\text{m} \times 1\ \text{mm s}^{-1} = 8.4 \times 10^{-12}\ \text{N}$$

This force corresponds to a displacement in the trap of:

$$F_{\text{Trap}} = k_{\text{Trap}} \times \Delta x = 50\ \text{pN}\ \mu\text{m}^{-1} \times \Delta x = 8.4 \times 10^{-12}\ \text{N}$$

$$\Delta x = 0.17\ \mu\text{m}$$

8.11 One possibility is to attach myosin dimers to a sphere that carries myosin antibodies and that is suitable for trapping in optical tweezers (see figure below). Then one can approach this sphere with a biotinylated actin filament using the tweezers, which are themselves immobilized on a biotinylated coverslip via avidins. A binding between the actin filament and the myosin can be detected by a counterforce that is generated by pulling the sphere away from the filament and detected by the tweezers set-up. If then power strokes are induced by ATP, for example, the corresponding forces can be detected by the optical tweezers.

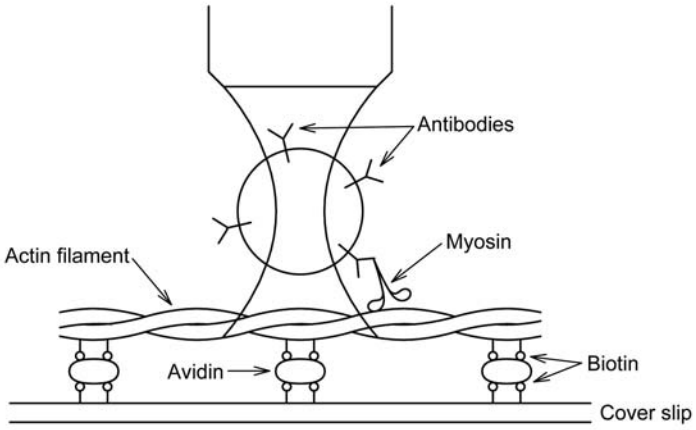

8.12 If several ligands are be linked to the cantilever this would be indicated by more than one spike in the force–distance diagram that would occur more or less reproducibly when approaching and removing several times the cantilever to and from the surface. The exact shape of these curves, however, will vary depending on the exact binding pairs and certainly not all ligands will always bind in each approaching and removing cycle.

8.13 When pulling relatively slowly, then the breaking of the binding often occurs at smaller forces than when pulling faster. When pulling faster a biotin bound to avidin, for example, then the avidin has less time to respond structurally to the pulling of the biotin out of the binding pocket and thus bond breakage occurs more abruptly at higher forces. When pulling very slowly even very strong bonds, such as biotin–avidin binding, can break at low forces.

8.14 An inside out patch configuration is more advantageous to investigate the influence of the ligand concentration on an intracellular ligand-gated ion channel because it is easy to control the ligand concentration in the exterior solution. In a similar manner an outside out patch configuration is more advantageous to investigate the influence of the ligand concentration on an extracellular ligand-gated ion channel.

8.15 The resistance can be calculated according to the following electric circuit.

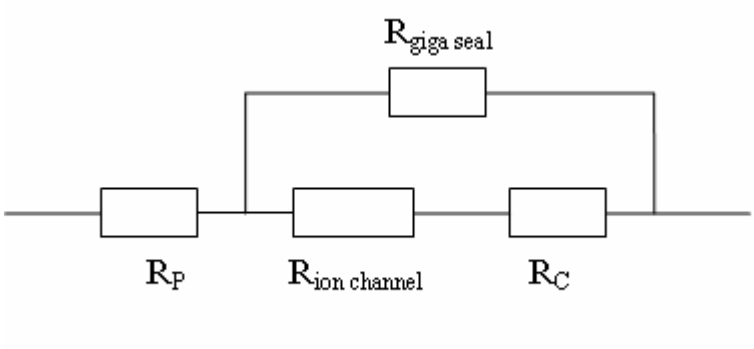

The electric circuit can be simplified as the following:

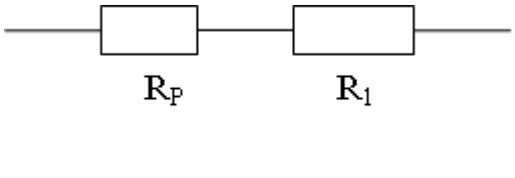

The resistance of R_1 is:

$$R_1^{-1} = \left(R_{\text{ion channel}} + R_C\right)^{-1} + R_{\text{giga seal}}^{-1}$$

$$R_1^{-1} = \frac{R_{\text{giga seal}} + R_{\text{ion channel}} + R_C}{\left(R_{\text{ion channel}} + R_C\right) \times R_{\text{giga seal}}}$$

$$R_1 = \frac{\left(R_{\text{ion channel}} + R_C\right) \times R_{\text{giga seal}}}{R_{\text{giga seal}} + R_{\text{ion channel}} + R_C}$$

The total resistance is therefore:

$$R_{\text{total}} = R_P + R_1 = R_P + \frac{\left(R_{\text{ion channel}} + R_C\right) \times R_{\text{giga seal}}}{R_{\text{giga seal}} + R_{\text{ion channel}} + R_C}$$

The resistance of the ion channel is:

$$R_{\text{ion}} = \frac{U}{I} = \frac{10\ \text{mV}}{10\ \text{pA}} = 10^9\ \Omega .$$

Consequently, the giga seal must have a resistance of at least:

$$R_{\text{giga}} \geq 10 \times R_{\text{ion}} = 10^{10}\ \Omega .$$

Chapter 9

9.1 The time gap between the pulses is:

$\frac{1}{80\ \text{MHz}} = 12.5\ \text{ns}$ (see figure);

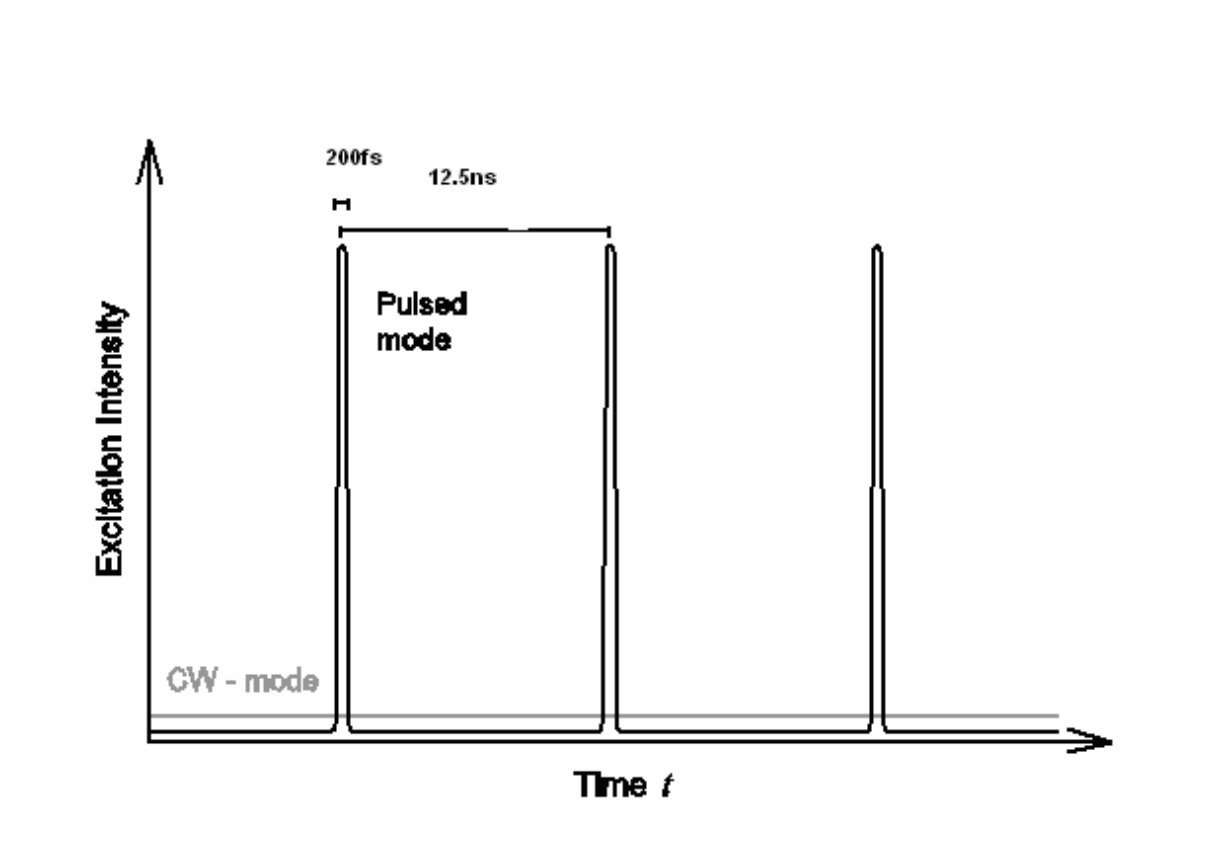

As a consequence the intensity during a 200 fs pulse is :

$\frac{I_{\text{Excitation}}^{\text{TPE}}}{I_{\text{Excitation}}^{\text{OPE}}} = \frac{12.5\ \text{ns}}{200\ \text{fs}} = 62500$ higher than in the CW mode.

The corresponding probability for two-photon excitation during a pulse is thus:

$\frac{P^{\text{TPE}}}{P^{\text{OPE}}} = \left(\frac{I_{\text{Excitation}}^{\text{TPE}}}{I_{\text{Excitation}}^{\text{OPE}}} \right)^2 = 62500^2$ times higher than in the CW mode.

However, during the CW mode the sample is irradiated:

$\frac{\text{CW}}{\text{Pulsed}} = \frac{12.5\ \text{ns}}{200\ \text{fs}} = 62500$ times longer.

As a consequence the average probability of two-photon excitation during longer periods is 62500 times higher in the pulsed mode than in the CW mode.

9.2 The dichroic mirror necessary for a two-photon excitation, dual colour confocal set-up is significantly simpler than the corresponding dichroic mirror for a one-photon excitation, dual colour confocal set-up (question 8.7, Chapter 8). It must only reflect all wavelengths in the infrared excitation regime (700–1200 nm) and transmit fluorescence in the visible range (~400–700 nm, compare also with the figure below). The dichroic mirror can be used for all fluorescence markers and two-photon excitation wavelengths. This is a great advantage of two-photon excitation, dual colour confocal microscopy over one-photon excitation, dual colour confocal microscopy in which each pair of fluorescence dyes requires the alignment of a different, expensive dichroic mirror. Often even the individual filters for the two fluorescence markers can be omitted when using a single filter that blocks efficiently the two-photon excitation wavelength. Since also no pinhole is necessary in two-photon microscopy the alignment is a lot easier when changing fluorescence dyes.

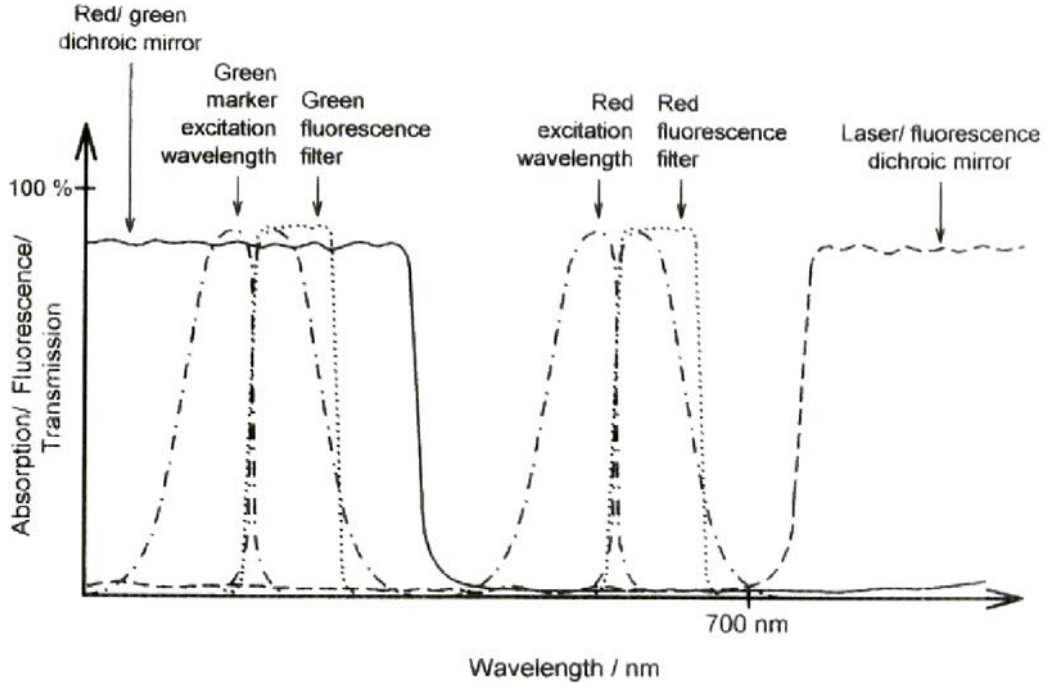

9.3 This can be proved by measuring a conventional one-photon absorption spectrum of carotenoids. As can be seen from Figure 9.6 there is no adsorption at around 600 nm at all, which is the region where a one-photon absorption into the first excited state of carotenoids would appear.

9.4 For two-photon excitation the dependence of the excitation probability for molecules with a transition dipole moment having an angle θ relative to the z axis is:

$$P_{\text{exc}}(\theta) \propto \cos^4 \theta$$

because two photons must be absorbed and the probabilities of two events that are required so that a process occurs must be multiplied to calculate the probability for the process (cf. Equations 3.7 and 9.2). As a consequence, the shape of the graphical presentation of the excitation probability analogous to figure 3.11 for two-photon excitation looks visually similar as figure 3.11 but is compressed in the x direction. Therefore, using two-photon excitation more molecules have a narrower angle with the z axis as in the case of one-photon

excitation and the maximum anisotropy, r_0^{TPE}, is larger than r_0. From the angle-θ-dependent excitation probability for two-photon excitation the maximum anisotropy, r_0^{TPE}, can be derived analogously as described in chapter 3 for one-photon excitation:

The number of molecules having the angle θ that are two-photon excited by the polarized light is: $f(\theta)\,\mathrm{d}\theta = \cos^4\theta \sin\theta\,\mathrm{d}\theta$.

The maximum fluorescence anisotropy for two-photon excitation can then be calculated by:

$$r_0^{\mathrm{TPE}} = \frac{\int_0^{\pi} f(\theta) r(\theta)\,\mathrm{d}\theta}{\int_0^{\pi} f(\theta)\,\mathrm{d}\theta} = \frac{\int_0^{\pi} \cos^4\theta \sin\theta \frac{3\cos^2\theta - 1}{2}\,\mathrm{d}\theta}{\int_0^{\pi} \cos^4\theta \sin\theta\,\mathrm{d}\theta} = \frac{\frac{1}{2}\int_0^{\pi} 3\cos^6\theta \sin\theta\,\mathrm{d}\theta - \frac{1}{2}\int_0^{\pi} \cos^4\theta \sin\theta\,\mathrm{d}\theta}{\int_0^{\pi} \cos^4\theta \sin\theta\,\mathrm{d}\theta}$$

$$u = \cos\theta$$

$$\frac{\mathrm{d}u}{\mathrm{d}\theta} = -\sin\theta$$

$$\mathrm{d}u = -\sin\theta\,\mathrm{d}\theta$$

$$\int_0^{\pi} 3\cos^6\theta \sin\theta\,\mathrm{d}\theta = \int_1^{-1} -3u^6\,\mathrm{d}u = -3\int_1^{-1} u^6\,\mathrm{d}u = \frac{6}{7}$$

$$\int_0^{\pi} \cos^4\theta \sin\theta\,\mathrm{d}\theta = -\int_1^{-1} u^4\,\mathrm{d}u = \frac{2}{5}$$

Solving this integration gives:

$$r_0^{\mathrm{TPE}} = \frac{\frac{1}{2}\times\frac{6}{7} - \frac{1}{2}\times\frac{2}{5}}{\frac{2}{5}} = \frac{4}{7}$$

For three-photon excitation the corresponding excitation probability is $P_{\mathrm{exc}}(\theta) \propto \cos^6\theta$ and the number of molecules having the angle θ that are three-photon excited by the polarized light is then:

$f(\theta)\,\mathrm{d}\theta = \cos^6\theta \sin\theta\,\mathrm{d}\theta$. As a consequence the photoselection for three-photon excitation is even more selective with respect to derivations of the angle θ from the z-axis and the maximum fluorescence anisotropy is even larger than using two-photon or one-photon excitation.

The maximum fluorescence anisotropy for three-photon excitation is then:

$$r_0^{\mathrm{3PE}} = \frac{\int_0^{\pi} f(\theta) r(\theta)\,\mathrm{d}\theta}{\int_0^{\pi} f(\theta)\,\mathrm{d}\theta} = \frac{\int_0^{\pi} \cos^6\theta \sin\theta \frac{3\cos^2\theta - 1}{2}\,\mathrm{d}\theta}{\int_0^{\pi} \cos^6\theta \sin\theta\,\mathrm{d}\theta} = \frac{\frac{1}{2}\int_0^{\pi} 3\cos^8\theta \sin\theta\,\mathrm{d}\theta - \frac{1}{2}\int_0^{\pi} \cos^6\theta \sin\theta\,\mathrm{d}\theta}{\int_0^{\pi} \cos^6\theta \sin\theta\,\mathrm{d}\theta}$$

$$u = \cos\theta$$
$$\frac{\mathrm{d}u}{\mathrm{d}\theta} = -\sin\theta$$
$$\mathrm{d}u = -\sin\theta\,\mathrm{d}\theta$$

$$\int_0^{\pi} 3\cos^8\theta\sin\theta\,\mathrm{d}\theta = \int_1^{-1} -3u^8\,\mathrm{d}u = -3\int_1^{-1} u^8\,\mathrm{d}u = \tfrac{2}{3}$$
$$\int_0^{\pi} \cos^6\theta\sin\theta\,\mathrm{d}\theta = -\int_1^{-1} u^6\,\mathrm{d}u = \tfrac{2}{7}$$

$$r_0^{\mathrm{3PE}} = \frac{\frac{1}{2}\times\frac{2}{3} - \frac{1}{2}\times\frac{2}{7}}{\frac{2}{7}} = \tfrac{2}{3}\,.$$

9.5 (a) Using Equation 9.3, $\nu_{\mathrm{Transition}} = \nu_1 + \nu_2$, we obtain for the wavelength of the generated light:

$$\frac{c}{\lambda_{\mathrm{Transition}}} = \frac{c}{\lambda_1} + \frac{c}{\lambda_2}$$

$$\frac{1}{\lambda_{\mathrm{Transition}}} = \frac{1}{\lambda_1} + \frac{1}{\lambda_2}$$

$$\lambda_{\mathrm{Transition}} = \frac{\lambda_1\lambda_2}{\lambda_1 + \lambda_2}$$

$$\lambda_{\mathrm{Transition}} = \frac{600\ \mathrm{nm}\times 1200\ \mathrm{nm}}{600\ \mathrm{nm} + 1200\ \mathrm{nm}} = 400\ \mathrm{nm}$$

(b) According to Equation 9.4 the probability is:

$$P_{\mathrm{Absorption}}^{\mathrm{Two\text{-}photon}} \propto I_{\mathrm{Excitation}}^{600\ \mathrm{nm}} \times I_{\mathrm{Excitation}}^{1200\ \mathrm{nm}}\,.$$

(c) This can be achieved by significantly lowering the intensity of the 600 nm light and increasing the intensity of the 1200 nm light by the same factor. According to $P_{\mathrm{Absorption}}^{\mathrm{Two\text{-}photon}} \propto I_{\mathrm{Excitation}}^{600\ \mathrm{nm}} \times I_{\mathrm{Excitation}}^{1200\ \mathrm{nm}}$ the overall probability for two-photon excitation with 600 *and* 1200 nm photon remains the same but the probability for two-photon excitation with two 600 nm photons decreases by the square of the factor by which the 600 nm light intensity has been decreased.

9.6 The dominating sum frequency is:

$$\nu_{\mathrm{wave\text{-}mixing}} = \nu_1 + \nu_2$$

$$\nu_{\text{wave-mixing}} = \frac{c}{\lambda_1} + \frac{c}{\lambda_2} = \left(\frac{1}{600\ \text{nm}} + \frac{1}{1200\ \text{nm}} \right) \times 3 \cdot 10^8\ \text{ms}^{-1} = 7.5 \times 10^{14}\ \text{s}^{-1}$$

The direction of the resulting field can be calculated by a vector addition of the photon wave vectors of the incoming photons. The absolute value of wave vector of a photon is:

$$\left| \vec{k} \right| = \frac{2\pi}{\lambda}$$

The corresponding value for 600 nm photons is therefore:

$$\left| \vec{k}_{600\ \text{nm}} \right| = \frac{2\pi}{600\ \text{nm}} = 1.05 \times 10^7\ \text{m}^{-1}$$

For 1200 nm photons:

$$\left| \vec{k}_{1200\ \text{nm}} \right| = \frac{2\pi}{1200\ \text{nm}} = 5.23 \times 10^6\ \text{m}^{-1}$$

The vector of the generated light is therefore:

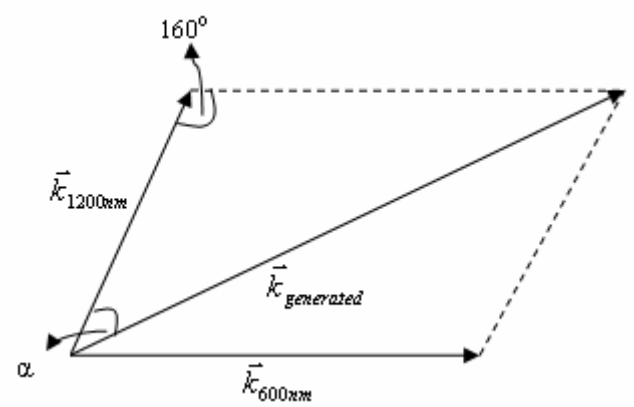

The absolute value of wave vector of the generated light beam:

$$\left| \vec{k}_{generated} \right| = \sqrt{\left| \vec{k}_{600nm} \right|^2 + \left| \vec{k}_{1200nm} \right|^2 - 2 \cdot \left| \vec{k}_{600nm} \right| \cdot \left| \vec{k}_{1200nm} \right| \cdot \cos 160°}$$

$$\left| \vec{k}_{generated} \right| = 1.55 \cdot 10^7\, m^{-1}$$

The angle relative to the 1200 nm beam can be calculated according to:

$$\frac{\sin 160^\circ}{\left| \vec{k}_{\text{generated}} \right|} = \frac{\sin \alpha}{\left| \vec{k}_{600\ \text{nm}} \right|}$$

$$\sin\alpha = \left|\vec{k}_{600nm}\right| \cdot \frac{\sin 160°}{\left|\vec{k}_{generated}\right|} = 0.233$$

$\alpha = \arcsin 0.233 = 13.4°$
The generated light beam has an angle of 13.4° relative to the 1200 nm beam.

9.7 The wavelength can be calculated according to:

$$v_{\text{Anti-Stokes}} = 2 \cdot v_{\text{Pump}} - v_{\text{Stokes}}$$

$$\frac{c}{\lambda_{\text{Anti-Stokes}}} = \frac{2c}{\lambda_{\text{Pump}}} - \frac{c}{\lambda_{\text{Stokes}}}$$

$$\frac{1}{\lambda_{\text{anti-Stokes}}} = \frac{2}{\lambda_{\text{pump}}} - \frac{1}{\lambda_{\text{Stokes}}}$$

$$\lambda_{\text{anti-Stokes}} = \frac{\lambda_{\text{pump}}\lambda_{\text{Stokes}}}{2\lambda_{\text{Stokes}} - \lambda_{\text{pump}}} = \frac{800\text{ nm} \times 870\text{ nm}}{2 \times 870\text{ nm} - 800\text{ nm}} = 740.4\text{ nm}$$

Again, the resulting vectors are calculated by vector addition. The absolute value of the wave vectors is:

$$\left|\vec{k}\right| = \frac{2\pi}{\lambda}$$

$$\left|\vec{k}_{\text{pump}}\right| = \frac{2\pi}{800\text{ nm}} = 7.85 \times 10^{6}\ \text{m}^{-1}$$

$$\left|\vec{k}_{\text{Stokes}}\right| = \frac{2\pi}{870\text{ nm}} = 7.22 \times 10^{6}\ \text{m}^{-1}$$

In CARS, two directions of anti-Stokes signals are generated:

$$\vec{k}_{\text{anti-Stokes}} = 2\vec{k}_{\text{pump}} - \vec{k}_{\text{Stokes}}$$

$$\vec{k}_{\text{anti-Stokes}} = -\left(2\vec{k}_{\text{pump}} - \vec{k}_{\text{Stokes}}\right)$$

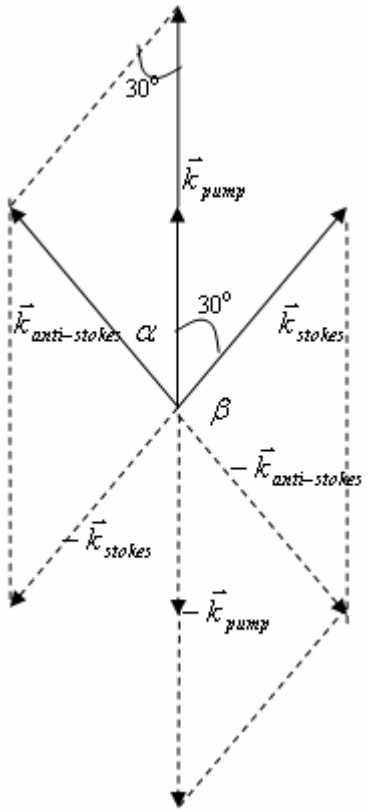

$$\left|\vec{k}_{\text{anti-Stokes}}\right| = \sqrt{4\times\left|\vec{k}_{\text{pump}}\right|^2 + \left|\vec{k}_{\text{Stokes}}\right|^2 - 2\times\left|\vec{k}_{\text{pump}}\right|\times\left|\vec{k}_{\text{Stokes}}\right|\times\cos 30^{\text{o}}}$$

$$\left|\vec{k}_{\text{anti-Stokes}}\right| = 3.95\times10^{6}\ \text{m}^{-1}$$

$$\frac{\sin 30^{\text{o}}}{\left|\vec{k}_{\text{anti-Stokes}}\right|} = \frac{\sin\alpha}{\left|\vec{k}_{\text{Stokes}}\right|}$$

$$\sin\alpha = \left|\vec{k}_{\text{Stokes}}\right|\times\frac{\sin 30^{o}}{\left|\vec{k}_{\text{anti-Stokes}}\right|} = 0.91$$

$$\alpha = \sin^{-1} 0.91 = 66.1^{\text{o}}$$

$$\beta = 180^{\text{o}} - 30^{\text{o}} - \alpha = 83.9^{\text{o}}$$

The wave vector of $\vec{k}_{\text{anti-Stokes}}$ has an angle of 66.1^{o} relative to the $\vec{k}_{\text{pump}}$. The opposite direction of $\vec{k}_{\text{anti-Stokes}}$ has an angle of 83.9^{o} relative to the $\vec{k}_{\text{Stokes}}$.

9.8 Here

$$\Phi_{\text{ET}} = \frac{{R_0}^6}{{R_0}^6 + r^6}$$

$$\Phi_{\mathrm{ET}} = \frac{(10\ \mathrm{nm})^6}{(10\ \mathrm{nm})^6 + (1.43\ \mathrm{nm})^6} = 0.99999145$$

$$\Phi_{\mathrm{ET}} = \frac{k_{\mathrm{ET}}}{\tau_{\mathrm{S_1}}^{-1} + k_{\mathrm{ET}}}$$

$$\Phi_{\mathrm{ET}} \times \tau_{\mathrm{S_1}}^{-1} + \Phi_{\mathrm{ET}} \times k_{\mathrm{ET}} = k_{\mathrm{ET}}$$

$$k_{\mathrm{ET}} = \frac{\Phi_{\mathrm{ET}} \times \tau_{\mathrm{S_1}}^{-1}}{(1 - \Phi_{\mathrm{ET}})} = \frac{0.99999145 \times (6\ \mathrm{ns})^{-1}}{(1 - 0.99999145)} = 1.95 \times 10^{13}\ \mathrm{s}^{-1}$$

In β-carotene the blue adsorption is entirely due to the $S_0 \rightarrow S_2$ transition because the $S_0 \rightarrow S_1$ transition is optically forbidden. But the molecules can relax to the S_1 state by internal conversion. Energy transfer between β-carotene and chlorophyll *a* can occur from the S_2 state to chlorophyll and from the S_1 state to chlorophyll. Since the latter corresponds to a dipole forbidden transition in the donor it is much slower than the transfer from the S_2 state.

9.9 The quantum efficiency for a single energy transfer step is:

$$\Phi_{ET} = \frac{k_{ET}}{\tau_{S_1}^{-1} + k_{ET}} = \frac{\tau_{ET}^{-1}}{\tau_{S_1}^{-1} + \tau_{ET}^{-1}} = \frac{(100\,fs)^{-1}}{(50ns)^{-1} + (100\,fs)^{-1}} = 0.99998\,.$$

Therefore, the total quantum efficiency of energy transfer over ten pigments is:

$$(\Phi_{ET})^{10} = \left(\frac{\tau_{ET}^{-1}}{\tau_{S_1}^{-1} + \tau_{ET}^{-1}} \right)^{10} = 0.9998$$

9.10 The energy loss corresponds to:

$$E_1 = h\nu_1$$
$$E_2 = h\nu_2$$
$$\Delta E = h\nu_1 - h\nu_2$$

Where E_1 is the energy of the absorbed photon and E_2 the energy of that can be donated by the chlorophyll. From these energies the energy loss can be calculated:

$$\frac{\Delta E}{E_1} = \frac{h\nu_1 - h\nu_2}{h\nu_1} = \frac{\nu_1 - \nu_2}{\nu_1} = \frac{c/\lambda_1 - c/\lambda_2}{c/\lambda_1} = \frac{\lambda_2 - \lambda_1}{\lambda_2} = \frac{690\ \mathrm{nm} - 480\ \mathrm{nm}}{690\ \mathrm{nm}} = 0.3$$

Chapter 10

10.1 The biggest advantage of quantum dots is that they have a higher photostability and achievable particle brightness. In addition, their fluorescence spectrum is narrower than the fluorescence spectrum of traditional fluorescence dyes. As a consequence a larger number of different quantum dots can be separately distinguished in fluorescence experiments in comparison to fluorescence dyes. Finally, the broad absorption spectra of quantum dots means that they can be excited simultaneously with a single excitation wavelength in the blue spectral region. A disadvantage of quantum dots is that they are significantly bigger than conventional fluorescence dyes. Therefore, quantum dots potentially influence the biochemical properties of labelled biomolecules to a larger extent.

10.2 Surface plasmon resonance (SPR) detection is advantageous if, for example, very sensitive binding and dissociation kinetics of protein ligands to receptors are to be analyzed or if unpurified cell extracts are to be analysed for the presence of the receptor. Then a small ligand can be immobilized on the device and the presence of the unlabelled receptor will be indicated by an SPR response. Using SPR, the ligands attached to the gold surface can be reused several times after appropriate washing steps. One advantage of measuring the fluorescence polarization anisotropy (FPA) is that, usually, a measurement takes significantly less time. This can be utilized, for example, in high-throughput screening where measurement times per sample well below 1 s might be necessary. If the assay principle is based on a competition assay, as outlined in Figures I.1 and I.2 of the Introduction to the book, then also many different small ligands that are not labelled can be tested. SPR is not very sensitive if a large receptor is immobilized on the surface to test the binding of different small ligands. The read-out of FPA is very robust and quantitative if it is important to detect small differences of the binding affinity between different ligands. A drawback of such a competitive FPA assay is that only binding to the specific binding site at which the labelled competitor binds can be measured – if the ligand to be tested binds only at other positions of the receptor then a binding will only be indicated by SPR.

10.3 The probabilities can be calculated according to a binomial distribution:

$$\Pr = \frac{n!}{k!(n-k)!} p^k (1-p)^{n-k}$$

For our problem n represents the number of DNA bases, k the number of errors and p the probability for a false read-out of a single base.

The probability that no error occurs is:
$(1-0.0001)^{1000} = 0.905$,

that one error occurs is:
$1000 \times 0.0001 \times (1-0.0001)^{999} = 0.09$

and that one or more errors occur is:
$1 - 0.905 = 0.095$.

10.4 It might well be that labelling with a green marker of, for example, cDNA 2 in Figure 10.10 is less efficient than cDNA 1. However, when using the same labelling chemistry the labelling with the red marker is usually to a similar extent more efficient for cDNA 1 in comparison to cDNA 2. As a result the relative comparison of red- or green-labelled cDNA is more or less unaffected for a distinct spot.

10.5 If knowledge about the location and presence of certain, known DNA sequences, which encode, for example, specific proteins, in chromosomes or in a larger genome is required, fluorescence *in situ* hybridization is a quick and reliable method for this purpose. If the entire sequence of a distinct DNA, which is completely unknown, is to be determined, the more time-consuming DNA sequencing technique has to be applied.

Chapter 11

11.1 (a) By a competitive binding assay, as illustrated in Figures I.1 and I.2 of the Introduction to the book. When a compound is capable of binding more strongly to the receptor than the natural labelled ligand then the labelled ligand will be forced out of the binding site. This can be measured by the changing fluorescence polarization, fluorescence correlation curves and sometimes also fluorescence lifetime.

(b) The assay quality can be quantified using the *Z′*-factor:

$Z' = 1 - 3\dfrac{\delta^+ + \delta^-}{\left|\bar{x}^+ - \bar{x}^-\right|}$, Equation 11.4.

From the values given in the table the fluorescence polarization has a Z′-factor of:

$$Z' = 1 - 3 \times \frac{0.001 + 0.001}{\left|0.01 - 0.1\right|} = 1 - 3 \times \frac{0.002}{0.09} = 0.93$$

The corresponding value for the fluorescence correlation assay is:

$$Z' = 1 - 3 \times \frac{100 + 100}{\left|80 - 500\right|} = 1 - 3 \times \frac{200}{420} = -0.43$$

and for the fluorescence lifetime assay:

$$Z' = 1 - 3 \times \frac{0.1 + 0.1}{\left|4.3 - 3.1\right|} = 1 - 3 \times \frac{0.2}{1.2} = 0.5$$

As a consequence, the fluorescence polarization assay is the best suited for the high-throughput screen.

11.2 The maximum number that can be tested in one day when a single measurement takes 100 ms is:

$$\frac{24\ \text{h} \times 60\ \text{min/ h} \times 60\ \text{s / min}}{100\ \text{ms}} = 864000\,.$$

This corresponds to uHTS.

From Figure 11.2 we can deduce that the necessary volume of solvent using 1536-well plates would be:
$864000 \times 10\ \mu\text{L} = 8.6\ \text{L}$

for 384-well plates already
$864000 \times 80\ \mu\text{L} = 69.1\ \text{L}$

and for 96-well plates even:
$864000 \times 200\ \mu\text{L} = 172.8\ \text{L}$.

11.3 When the assay quality is limited by the shot noise, the standard deviation of the photon noise is equal to the square root of the average number of photons: $\delta = \sqrt{N}$.

We assume that for the 1 s measuring time the assay quality is almost exclusively limited by the shot noise:

$$Z'_{1s} = 1 - 3 \times \frac{\delta^+_{1s} + \delta^-_{1s}}{\left|\bar{X}^+_{1s} - \bar{X}^-_{1s}\right|} = 1 - 3 \times \frac{\sqrt{2\bar{X}^-_{1s}} + \sqrt{\bar{X}^-_{1s}}}{\left|2\bar{X}^-_{1s} - \bar{X}^-_{1s}\right|} = 0.4$$

$$1 - 3 \times \frac{\left(\sqrt{2}+1\right)\sqrt{\bar{X}^-_{1s}}}{\bar{X}^-_{1s}} = 0.4$$

$$3 \times \frac{\left(\sqrt{2}+1\right)}{\sqrt{\bar{X}^-_{1s}}} = 0.6$$

$$\sqrt{\bar{X}^-_{1s}} = \frac{\left(\sqrt{2}+1\right)}{0.2}$$

$$\bar{X}^-_{1s} = \left[5 \times \left(\sqrt{2}+1\right)\right]^2 = 145.7$$

When we assume that for the 3 s measuring time the assay quality is also exclusively limited by the shot noise the Z'-factor can be calculated as follows:

$$Z'_{3s} = 1 - 3 \times \frac{\delta^+_{3s} + \delta^-_{3s}}{\left|\bar{X}^+_{3s} - \bar{X}^-_{3s}\right|} = 1 - 3 \times \frac{\sqrt{3\bar{X}^+_{1s}} + \sqrt{3\bar{X}^-_{1s}}}{\left|3\bar{X}^+_{1s} - 3\bar{X}^-_{1s}\right|} = 1 - 3 \times \frac{\sqrt{6\bar{X}^-_{1s}} + \sqrt{3\bar{X}^-_{1s}}}{\left|6\bar{X}^-_{1s} - 3\bar{X}^-_{1s}\right|} = 1 - \frac{\left(\sqrt{6}+\sqrt{3}\right)\sqrt{\bar{X}^-_{1s}}}{\bar{X}^-_{1s}}$$

We know that $\bar{X}^-_{1s} = 145.7$:

$$Z'_{3s} = 1 - \frac{\left(\sqrt{6}+\sqrt{3}\right)\sqrt{\bar{X}^-_{1s}}}{\bar{X}^-_{1s}} = 1 - \frac{\left(\sqrt{6}+\sqrt{3}\right)\sqrt{145.7}}{145.7} = 0.65$$

Similarly, for the 9 s measuring time the Z'-factor would be:

$$Z'_{9s} = 1 - 3 \times \frac{\delta^+_{9s} + \delta^-_{9s}}{s\left|\bar{X}^+_{9s} - \bar{X}^-_{9s}\right|} = 1 - 3 \times \frac{\sqrt{9\bar{X}^+_{1s}} + \sqrt{9\bar{X}^-_{1s}}}{\left|9\bar{X}^+_{1s} - 9\bar{X}^-_{1s}\right|} = 1 - 3 \times \frac{\sqrt{18\bar{X}^-_{1s}} + \sqrt{9\bar{X}^-_{1s}}}{\left|18\bar{X}^-_{1s} - 9\bar{X}^-_{1s}\right|} = 1 - 3 \times \frac{\left(\sqrt{18}+\sqrt{9}\right)\sqrt{\bar{X}^-_{1s}}}{9\bar{X}^-_{1s}}$$

$$\bar{X}^-_{1s} = 145.7$$

$$Z'_{9\,\mathrm{s}} = 1 - 3 \times \frac{\left(\sqrt{18} + \sqrt{9}\right)\sqrt{\bar{\bar{X}}_{1\,\mathrm{s}}^{-}}}{9\bar{\bar{X}}_{1\,\mathrm{s}}^{-}} = 1 - 3 \times \frac{3 \times \left(\sqrt{2} + 1\right)\sqrt{\bar{\bar{X}}_{1\,\mathrm{s}}^{-}}}{9\bar{\bar{X}}_{1\,\mathrm{s}}^{-}} = 1 - \frac{\left(\sqrt{2} + 1\right)\sqrt{145.7}}{145.7} = 0.80$$

The corresponding factors are summarized in the following table:

Z' factor	Experimental Z' factor	Theoretical Z' factor
$Z'_{1\,\mathrm{s}}$	0.4	0.4
$Z'_{3\,\mathrm{s}}$	0.6	0.65
$Z'_{9\,\mathrm{s}}$	0.65	0.80

The 3 s measuring time would be a good choice in such a situation because it has a Z'-factor close to the maximum achievable value and requires 3-times less measuring time than necessary for the highest observed Z′-factor. One reason for the worse experimental Z'-factors might be statistical variations in the biological sample preparation, noise in the instrumentation or from the solvent. If higher Z′-factors are necessary and variations in the biological sample preparation are the reason then protocols must be developed that provide more homogenous samples. If noise from the instrumentation is the reason then, first, sources for the highest errors must found, for example pipetting uncertainties or detector noise, and then be improved or eliminated. A solution against solvent background would be a better filter system or different or purer solvents.